

UC Berkeley

UC Berkeley Previously Published Works

Title

Bacteria attenuation by iron electrocoagulation governed by interactions between bacterial phosphate groups and Fe(III) precipitates

Permalink

<https://escholarship.org/uc/item/27f797jr>

Authors

Delaire, Caroline
van Genuchten, Case M
Amrose, Susan E
[et al.](#)

Publication Date

2016-10-01

DOI

10.1016/j.watres.2016.07.020

Peer reviewed

Manuscript Number:

Title: Bacteria attenuation by iron electrocoagulation governed by interactions between bacterial phosphate groups and Fe(III) precipitates

Article Type: Research Paper

Keywords: Iron electrocoagulation; bacteria attenuation; bacterial surface functional groups; specific interactions; bivalent cations; oxyanions

Corresponding Author: Mrs. Caroline Delaire,

Corresponding Author's Institution: University of California, Berkeley

First Author: Caroline Delaire

Order of Authors: Caroline Delaire; Case M van Genuchten, PhD; Susan E Amrose, PhD; Ashok J Gadgil, PhD

Abstract: Iron electrocoagulation (Fe-EC) is a low-cost process in which Fe(II) generated from an Fe(0) anode reacts with dissolved O₂ to form (1) Fe(III) precipitates with an affinity for bacterial cell walls and (2) bactericidal reactive oxidants. Previous work suggests that Fe-EC is a promising treatment option for groundwater containing arsenic and bacterial contamination. However, the mechanisms of bacteria attenuation and the impact of major groundwater ions are not well understood. In this work, using the model indicator *Escherichia coli* (*E. coli*), we show that physical removal via enmeshment in EC precipitate flocs is the primary process of bacteria attenuation in the presence of HCO₃⁻, which significantly inhibits inactivation, possibly due to a reduction in the lifetime of reactive oxidants. We demonstrate that the adhesion of EC precipitates to cell walls, which results in bacteria encapsulation in flocs, is driven primarily by interactions between EC precipitates and phosphate functional groups on bacteria surfaces. In single solute electrolytes, both P (0.4 mM) and Ca/Mg (1-13 mM) interfered with the adhesion of EC precipitates to bacterial cell walls, whereas Si (0.4 mM) and ionic strength (2-200 mM) did not impact *E. coli* attenuation. Interestingly, P (0.4 mM) did not affect *E. coli* attenuation in electrolytes containing Ca/Mg, consistent with bivalent cation bridging between bacterial phosphate groups and inorganic P sorbed to EC precipitates. Finally, we found that EC precipitate adhesion is largely independent of cell wall composition, consistent with comparable densities of phosphate functional groups on Gram-positive and Gram-negative cells. Our results are critical to predict the performance of Fe-EC to eliminate bacterial contaminants from waters with diverse chemical compositions.

Suggested Reviewers: Shankar Chellam
Texas A&M University
chellam@tamu.edu

Dr. Chellam is an expert on water treatment technologies, and he has worked on iron and aluminum electrocoagulation for virus control.

Chuanyong Jing

Chinese Academy of Science

cyjing@rcees.ac.cn

Dr. Jing works on biogeochemistry and on environmental interfacial processes. He has recently co-authored a ATR-FTIR study about bacteria-goethite adhesion

Sharon Walker

University of California, Riverside

swalker@engr.ucr.edu

Dr. Walker is an expert on bacteria-particle adhesion in sub-surface environments, and on the role of cell surface polymers in bacteria adhesion and transport

Andreas Voegelin

EAWAG

andreas.voegelin@eawag.ch

Dr. Voegelin is an expert on molecular environmental geochemistry and on the reactivity of iron(III) precipitates and interactions with co-occurring ions.

Jon Chorover

University of Arizona

Chorover@email.arizona.edu

Dr. Chorover is an expert on the investigation of the interactions between iron oxides and bacterial cell walls using spectroscopic methods

Sanjay Mohanty

University of Pennsylvania

sanjay.mohanty@colorado.edu

Dr. Mohanty has worked on bacteria-mineral interactions in the context of bacteria transport in biofilters

Changa Lee

Ulsan National Institute of Science and Technology

clee@unist.ac.kr

Dr. Lee has worked on pathogen inactivation and on the production of reactive oxidants from zero-valent and ferrous iron

Mark van Loosdrecht
Department of Biochemical Engineering
Delft University of Technology
KWR Watercycle Research
Delft
Netherlands

April 21st, 2016

Dear *Water Research* Editor,

On behalf of all coauthors, I am pleased to submit our manuscript “Bacteria Attenuation by Iron Electrocoagulation Governed by Interactions between Bacterial Phosphate Groups and Fe(III) Precipitates” enclosed for consideration as a research paper for *Water Research*.

In this study, we investigate a specific application –bacteria attenuation- of iron electrocoagulation (Fe-EC), a promising technology for the treatment of arsenic-contaminated groundwater in low-resource settings. Simultaneous arsenic and bacteria attenuation in Fe-EC has been demonstrated in our previous study, and constitutes a significant advantage of this technology in areas where arsenic often concurs with fecal contamination. However, the processes leading to bacteria attenuation and the impact of groundwater composition are not well understood. This manuscript presents new results elucidating the molecular-scale mechanisms of bacteria attenuation in Fe-EC, and the role that major groundwater ions, such as HCO_3^- , P, Si, Ca and Mg, play in such mechanisms.

Our work goes beyond presenting remediation results because we thoroughly **investigate the processes** leading to bacteria inactivation and removal in Fe-EC. In addition, our findings have **significant implications for field treatment** as they allow to predict the performance of Fe-EC to attenuate various types of bacterial contamination in different groundwater matrices. We showed that attenuation is independent of cell wall composition, which is critical to generalize our findings to all bacterial species relevant to water quality. Finally, the molecular mechanisms identified in this study can be used to discuss the potential of Fe-EC, and other Fe-based coagulation processes, to treat various water sources, such as surface water, agricultural runoff and wastewater.

The results presented here are **novel**, as no other study to the authors’ knowledge has investigated the bacterial surface functional groups and the type of interaction involved in the adhesion of Fe(III) (oxyhydr)oxides to cell walls **in water matrices representative of field conditions**. Specifically, molecular-scale interactions between bacteria and Fe(III) oxides in systems containing bivalent cations and oxyanions, which alter the surface of bacterial cells and Fe(III) oxides, are not known.

Finally, we believe that our approach to elucidate bacteria-precipitates interactions is **innovative**. In systems where bacteria are encapsulated inside flocs and in the complex groundwater-like electrolytes, spectroscopic techniques such as ATR-FTIR cannot adequately determine bacterial functional groups mediating bacteria-precipitate adhesion. Instead, **we used a novel approach**, where macroscopic data of bacteria attenuation in systematically varied electrolytes was combined with ζ -potential measurements to elucidate molecular-scale processes. Building on previous spectroscopic studies in more simple controlled systems, our approach allowed us to gain knowledge on bacteria-Fe(III) precipitate interactions in complex water matrices.

We believe that this work will be relevant to a general audience interested in mechanistic aspects as well as in field applicability of drinking water treatment technologies.

Sincerely yours,

Caroline Delaire (corresponding author)
Department of Civil and Environmental Engineering
University of California, Berkeley
Berkeley, California, USA 94720
Phone: +1 (510) 417-9491
caroline.delaire@orange.fr

Case M. van Genuchten
Institut de Dynamiques de la Surface Terrestre
University of Lausanne
Lausanne, 1015-CH, Switzerland
cmvangenuchten@gmail.com

Susan E. Amrose
Department of Civil and Environmental Engineering
University of California, Berkeley
Berkeley, California, USA 94720
samrose@berkeley.edu

Ashok J. Gadgil
Energy Technologies Area
Lawrence Berkeley National Laboratory
Berkeley, California, USA 94720
ajgadgil@lbl.gov

Bacteria attenuation by iron electrocoagulation governed by interactions between bacterial phosphate groups and Fe(III) precipitates

Caroline Delaire^{*,†}, Case M. van Genuchten[§], Susan E. Amrose[†], Ashok J. Gadgil^{†,‡}

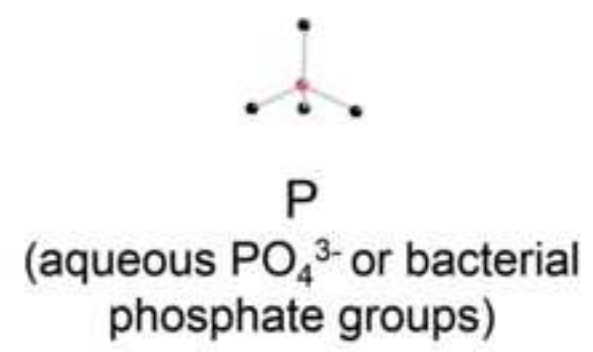
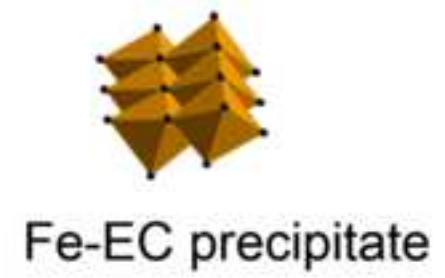
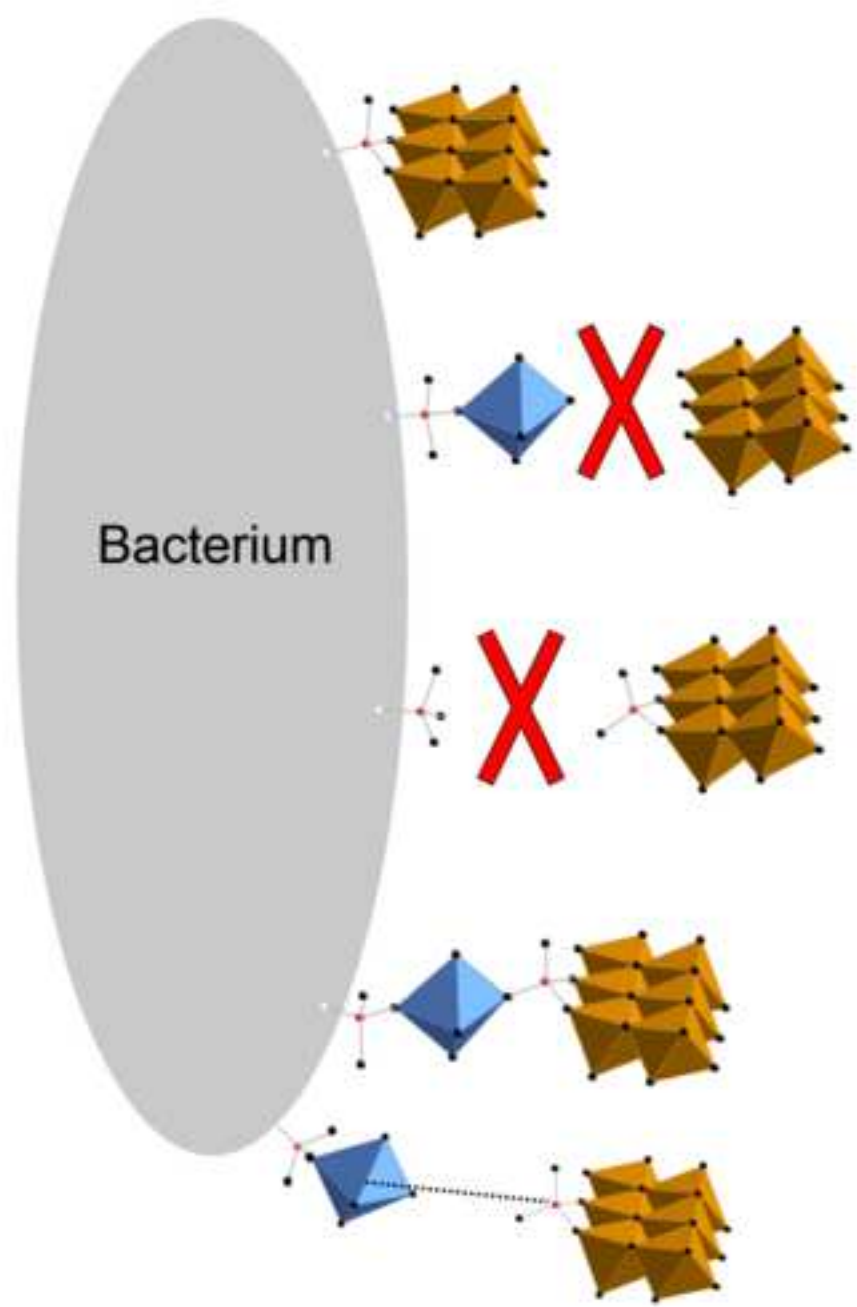
[†] Department of Civil and Environmental Engineering, University of California, Berkeley, California 94720-1710, United States

[§] Department of Earth Sciences – Geochemistry, Faculty of Geosciences, Utrecht University, Utrecht 3508TA, The Netherlands

[‡] Energy Technologies Area, Lawrence Berkeley National Laboratory, Berkeley, California 94720, United States

Highlights

- In natural waters, bacteria attenuation by Fe-EC is primarily due to physical removal with flocs
- Bacterial phosphate groups govern the adhesion of EC precipitates to cell walls
- Ca/Mg decrease removal, Si has no effect, and P decreases removal if Ca/Mg are absent
- Fe-EC is equally effective for Gram positive and negative (rough and smooth) strains



1 **Bacteria attenuation by iron electrocoagulation governed by interactions between bacterial**
2 **phosphate groups and Fe(III) precipitates**

3

4 Caroline Delaire^{*,†}, Case M. van Genuchten[§], Susan E. Amrose[†], Ashok J. Gadgil^{†,‡}

5

6

7

8

9

10 [†] Department of Civil and Environmental Engineering, University of California, Berkeley, California
11 94720-1710, United States

12

13 [§] Department of Earth Sciences – Geochemistry, Faculty of Geosciences, Utrecht University, Utrecht
14 3508TA, The Netherlands

15

16 [‡] Energy Technologies Area, Lawrence Berkeley National Laboratory, Berkeley, California 94720,
17 United States

18

19

20

21

22

23 * Corresponding author: Department of Civil and Environmental Engineering, University of California,
24 Berkeley, CA 94720-1710, United States. Phone: (+1) 510-417-9491; email: caroline.delaire@orange.fr

25

26

27

28

29 **Abstract**

30 Iron electrocoagulation (Fe-EC) is a low-cost process in which Fe(II) generated from an Fe(0) anode
31 reacts with dissolved O₂ to form (1) Fe(III) precipitates with an affinity for bacterial cell walls and (2)
32 bactericidal reactive oxidants. Previous work suggests that Fe-EC is a promising treatment option for
33 groundwater containing arsenic and bacterial contamination. However, the mechanisms of bacteria
34 attenuation and the impact of major groundwater ions are not well understood. In this work, using the
35 model indicator *Escherichia coli* (*E. coli*), we show that physical removal via enmeshment in EC
36 precipitate flocs is the primary process of bacteria attenuation in the presence of HCO₃⁻, which
37 significantly inhibits inactivation, possibly due to a reduction in the lifetime of reactive oxidants. We
38 demonstrate that the adhesion of EC precipitates to cell walls, which results in bacteria encapsulation in
39 flocs, is driven primarily by interactions between EC precipitates and phosphate functional groups on
40 bacteria surfaces. In single solute electrolytes, both P (0.4 mM) and Ca/Mg (1-13 mM) interfered with the
41 adhesion of EC precipitates to bacterial cell walls, whereas Si (0.4 mM) and ionic strength (2-200 mM)
42 did not impact *E. coli* attenuation. Interestingly, P (0.4 mM) did not affect *E. coli* attenuation in
43 electrolytes containing Ca/Mg, consistent with bivalent cation bridging between bacterial phosphate
44 groups and inorganic P sorbed to EC precipitates. Finally, we found that EC precipitate adhesion is
45 largely independent of cell wall composition, consistent with comparable densities of phosphate
46 functional groups on Gram-positive and Gram-negative cells. Our results are critical to predict the
47 performance of Fe-EC to eliminate bacterial contaminants from waters with diverse chemical
48 compositions.

49

50 **Keywords**

51 Iron electrocoagulation; bacteria attenuation; bacterial surface functional groups; specific interactions;
52 bivalent cations; oxyanions.

53 **Highlights**

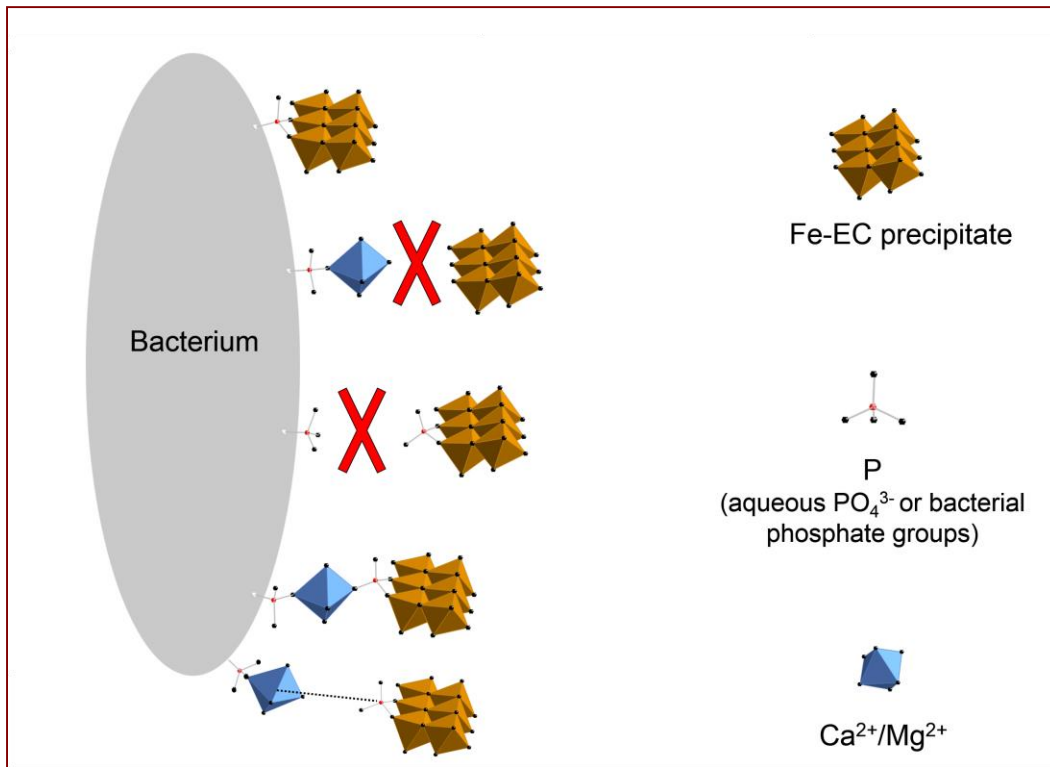
- 54 • In natural waters, bacteria attenuation by Fe-EC is primarily due to physical removal with flocs
- 55 • Bacterial phosphate groups govern the adhesion of EC precipitates to cell walls
- 56 • Ca/Mg decrease removal, Si has no effect, and P decreases removal if Ca/Mg are absent
- 57 • Fe-EC is equally effective for Gram positive and negative (rough and smooth) strains

58

59

60

61 **Graphical abstract**



62

63

64

65

66 **1. Introduction**

67 Iron electrocoagulation (Fe-EC) is a process relying on the electrolytic dissolution of an Fe(0) anode
68 to generate Fe(II), which is oxidized by dissolved O₂ to produce Fe(III) (oxyhydr)oxide precipitates with
69 an affinity for microbial and chemical contaminants (Delaire et al., 2015; van Genuchten et al., 2012). Fe-
70 EC can efficiently remove arsenic from contaminated groundwater (Amrose et al., 2014; Li et al., 2012),
71 and has also been shown to attenuate bacteria in a range of water matrices (Barrera-Díaz et al., 2003;
72 Delaire et al., 2015; Ghernaout et al., 2008). In a recent study, we demonstrated that Fe-EC can attenuate
73 *Escherichia coli* (*E. coli*) from synthetic Bengal groundwater (SBGW) without detriment to arsenic
74 removal (Delaire et al., 2015), confirming that Fe-EC has promising applications for low-cost
75 groundwater remediation (Amrose et al., 2014). Two processes contributed to bacteria attenuation in Fe-
76 EC: (1) physical removal, caused by bacteria enmeshment in Fe(III) flocs and subsequent settling, and (2)
77 inactivation by reactive species produced upon Fe(II) oxidation by O₂. Fundamental aspects of the
78 mechanisms underlying these two processes remain unknown. For example, the type of chemical
79 interactions governing bacteria enmeshment in flocs is not well understood. In addition, the effect of
80 major groundwater components, such as HCO₃⁻, Ca, Mg, Si, and P, which can interfere with both
81 inactivation and removal, has not been investigated. Finally, the impact of bacteria surface structure
82 (Gram-positive versus Gram-negative, smooth versus rough Gram-negative) on attenuation has not been
83 elucidated. By addressing these knowledge gaps, this study can improve considerably our predictions of
84 Fe-EC performance in various water matrices containing different types of bacterial contamination.

85 Our previous work suggests that the adhesion of EC precipitates to cell walls is a key process in
86 bacteria enmeshment in flocs (Delaire et al., 2015). Specifically, the significantly higher bacteria removal
87 by Fe-EC in comparison to coagulation with pre-synthesized ferrihydrite (for the same Fe(III)
88 concentration) shows that removal cannot be solely attributed to the mechanical sweeping of bacterial
89 cells by Fe(III) flocs (sweep flocculation). In addition, increased removal at higher Fe dosages indicates a
90 stoichiometric relationship between Fe(III) precipitates and bacterial surfaces, consistent with the primary

91 role of precipitate adhesion to cell walls. However, important questions remain regarding the bacterial
92 functional groups involved in such adhesion, the type of interaction (electrostatic versus specific
93 bonding), and the effects of groundwater chemistry and cell wall structure.

94 Four types of surface functional groups are present on bacterial cell walls at comparable densities:
95 hydroxyl ($pK_a \sim 9.0$), amine ($pK_a \sim 9.0$), carboxyl ($pK_a \sim 4.7$), and phosphate groups ($pK_{a1} \sim 3.1$, $pK_{a2} \sim$
96 6.6) (Borrok et al., 2005; Ngwenya et al., 2003). Hydroxyl and amine moieties do not have a strong
97 affinity for Fe(III) oxides (McBride and Kung, 1991; Norén et al., 2008) and therefore they are not
98 expected to strongly interact with EC precipitates. By contrast, carboxyl and phosphate moieties have
99 strong affinities for Fe(III) oxides (Arai and Sparks, 2001; Chassé et al., 2015; Filius et al., 2000; van
100 Genuchten et al., 2014a) and studies using Attenuated Total Reflectance Fourier-Transform Infrared
101 spectroscopy (ATR-FTIR) have shown direct bonding of bacterial phosphate and carboxyl groups to
102 hematite and goethite (Elzinga et al., 2012; Parikh and Chorover, 2006; Parikh et al., 2014). However,
103 these studies were performed in controlled laboratory systems and simple water matrices, and they cannot
104 be directly extrapolated to Fe-EC in groundwater, where precipitates and bacteria interact in an agitated
105 suspension and in the presence of bivalent cations (Ca and Mg) and oxyanions (P and Si), which can sorb
106 to bonding sites on bacteria (Beveridge and Koval, 1981; Johnson et al., 2007) and precipitates (van
107 Genuchten et al., 2014b), respectively, and may therefore interfere with adhesion.

108 In addition to electrolyte composition, a number of studies have shown that the biomolecular structure
109 of bacterial cell walls can affect their interactions with mineral surfaces through changes in surface
110 charge, hydrophobicity and steric hindrance (Chen and Walker, 2012; Jacobson et al., 2015; Walker et al.,
111 2004). Because waterborne pathogenic bacteria and indicator organisms span the range of Gram-positive,
112 smooth and rough (with and without O-antigen) Gram-negative strains (WHO, 2011), understanding the
113 impact of cell wall structure on bacteria attenuation with Fe-EC is essential to generalize our findings to
114 all bacterial species relevant to water quality.

115 Spectroscopic techniques such as ATR-FTIR, X-ray fluorescence (XRF) and X-ray absorption
116 spectroscopy (XAS) have been used to study bacteria-Fe systems (Chan et al., 2009; Elzinga et al., 2012;
117 Miot et al., 2009; Yan et al., 2016). However, these techniques cannot adequately determine bacteria-
118 Fe(III) interactions in systems where Fe(III) is co-precipitated with bacteria in complex electrolytes
119 similar to groundwater. For example, P-Fe bonds from bacteria-precipitate interactions and from aqueous
120 P sorption to precipitates look very similar using ATR-FTIR (Elzinga et al., 2012) and would not be
121 distinguishable with P K-edge XAS (Kelly et al., 2008). Additionally, ATR-FTIR is not suited to
122 investigate interactions taking place inside large flocs due to the low penetration length of infrared beams
123 in aqueous medium ($\sim 1\mu\text{m}$). To circumvent these limitations, the present study proposes an innovative
124 approach, where macroscopic data of bacteria attenuation in systematically varied electrolytes are
125 combined with ζ -potential measurements to elucidate the molecular interactions between bacteria and EC
126 precipitates. Although this approach can only provide indirect evidence for specific interactions between
127 bacteria and precipitates, it builds upon previous spectroscopic studies, which have identified bacteria-Fe
128 oxide bonding processes in simple controlled systems (Elzinga et al., 2012; Parikh and Chorover, 2006;
129 Parikh et al., 2014) and structures of Fe-EC precipitates in complex water matrices (van Genuchten et al.,
130 2014a, 2014b), to gain information about bacteria removal mechanisms in groundwater-like electrolytes.

131 The goals of this study are to: (1) determine the impact of HCO_3^- , Ca, Mg, P and Si on bacteria
132 attenuation with Fe-EC, (2) identify the bacterial functional groups involved in the adhesion of EC
133 precipitates to cell walls and investigate the type of interaction (electrostatic versus specific), and (3) test
134 the generalizability of these conclusions to various bacteria types. To achieve these objectives, we first
135 compared Fe-EC with FeCl_3 coagulation to distinguish the contributions of inactivation and removal via
136 enmeshment in flocs to overall bacteria attenuation in Fe-EC as a function of the HCO_3^- concentration.
137 Inactivation results were confirmed using live-dead staining. Second, we systematically investigated the
138 effect of ionic strength, Ca/Mg and P/Si on *E. coli* attenuation, both in single and multiple solute
139 electrolytes, to constrain the bacterial functional groups involved in precipitate adhesion to cell walls. ζ -

140 potential, a proxy for surface charge, was used to assess the interaction of major groundwater ions with
141 the surface of EC precipitates or *E. coli* cells. Third, we validated our proposed mechanism with 3
142 bacteria strains bearing different surface structures (smooth and rough Gram-negative, and Gram-
143 positive). Our results strongly suggest that Fe-EC can be used to remove various types of bacteria from a
144 wide range of water matrices representative of regions affected by arsenic and microbial contamination of
145 drinking water sources. More generally, this study can help predict the performance of Fe-EC, and other
146 Fe-based coagulation processes, to reduce bacterial contaminants from drinking water and wastewater.

147

148 **2. Methods**

149 **2.1. Bacteria preparation and enumeration**

150 One Gram-positive and two Gram-negative bacterial strains were used: *Enterococcus faecalis* (ATCC
151 19433, no antibiotic resistance), *Escherichia coli* K12 (NCM 4236, kanamycin-resistant), and *Escherichia*
152 *coli* ECOR 10 (from STEC center, ampicillin-resistant (Mazel et al., 2000)). K12 is a rough strain (no O-
153 antigen) (Stevenson et al., 1994) whereas ECOR 10 is a smooth strain (O-antigen present, serotype O6)
154 (STEC center, 2016). After three propagations in growth media amended with appropriate antibiotics,
155 stationary-phase bacteria were rinsed 3 times and resuspended in 100 mM NaCl as detailed in the
156 Supporting Information. Bacteria were spiked in Fe-EC electrolytes to achieve initial concentrations of
157 $10^{6.1-6.7}$ CFU/mL ($10^{5.0-5.8}$ CFU/mL for *E. faecalis*). Bacteria concentrations were enumerated in duplicate
158 in 0.1 mL aliquots as colony forming units (CFU) using the spread plate technique on agar amended with
159 appropriate antibiotics (detection limit of 10 CFU/mL), as described in the Supporting Information.

160

161 **2.2. Electrolytes**

162 The list of electrolytes used in bacteria attenuation experiments is specified in Table S1. In summary,
163 we first varied the concentration of HCO_3^- (0.1-8.0 mM) to examine its impact on bacteria inactivation.

164 Second, a range of ionic strengths was investigated by varying NaCl (in deionized water and in SBGW)
165 or NaClO₄ (in 1 mM CaCl₂). Then, concentrations of bivalent cations (Ca: 0-13.5 mM and Mg: 0-10.6
166 mM) and oxyanions (P: 0-0.4 mM and Si: 0-0.4 mM) were systematically varied, in single and composite
167 electrolytes, to elucidate their effect on bacteria removal. Finally, SBGW containing 8.2 mM HCO₃⁻, 2.7
168 mM Ca, 2.0 mM Mg, 1.3 mM Si, 0.15 mM P, and 6.3 μM As(III), was prepared as described elsewhere
169 (Delaire et al., 2015) and used as the electrolyte in some experiments. All experiments were conducted at
170 pH 7.0 ± 0.3, except for the comparisons between the three bacterial strains, which were conducted at pH
171 7.5 ± 0.2. The pH was held constant throughout experiments by adding HCl, NaOH or NaHCO₃ as
172 needed. Electrolytes were selected in part to overlap with previous work on the structure of EC
173 precipitates (van Genuchten et al., 2014a, 2014b, 2012), which we leverage in our interpretations of
174 bacteria attenuation and ζ-potential measurements.

175

176 **2.3. Fe-EC and FeCl₃ experiments**

177 The procedure used for Fe-EC experiments has been described elsewhere (Delaire et al., 2015) and is
178 detailed in the Supporting Information. Briefly, two 1 cm × 8 cm Fe(0) electrodes were submerged in 200
179 mL of electrolyte spiked with bacteria (anodic submerged area of 3 cm²). In all experiments, a current
180 density of 10 mA/cm² was applied for 11 min, resulting in a Faradaic Fe dosage of 0.5 mM. After the
181 electrolysis stage, suspensions were stirred open to the atmosphere for 90-180 min to allow for complete
182 Fe(II) oxidation and formation of Fe(III) precipitates. Suspensions were then left to settle overnight to
183 separate individual cells from cells associated with EC precipitates. When required for floc formation and
184 settling (Table S1), 5 mg/L-Al of Al₂(SO₄)₃ (alum) was added at the end of the mixing period, along with
185 approximately 1.5 mM NaHCO₃ to avoid a pH drop. Preliminary tests confirmed that the addition of alum
186 did not significantly modify bacteria attenuation (see Supporting Information). Solution pH was not
187 controlled during the settling stage. In a subset of experiments, coagulation by FeCl₃ addition was used
188 instead of Fe-EC to isolate the contribution of removal from that of inactivation. In these experiments, 1

189 mL of a 100 mM FeCl₃ solution was added to the electrolyte and the solution pH, which dropped to ~3
190 during FeCl₃ addition, was re-adjusted to 7.0±0.1 in less than 5 min.

191 Unfiltered and filtered (0.45 µm nylon filters) samples were taken before Fe-EC, and before and after
192 overnight settling, for measurements of Fe, As, Ca, Mg, P, and Si by inductively coupled plasma optical
193 emission spectrometry (ICP–OES, PerkinElmer 5300 DV, measurement error typically < 5%). All
194 samples for ICP-OES analysis were digested in 0.2 M HCl. Filtered and unfiltered samples were used to
195 measure Fe(II) and total Fe (Fe(II) + Fe(III)), respectively (Delaire et al., 2015). Across the 113 bacteria
196 attenuation experiments reported here, the total Fe concentration after Fe-EC (Fe dosage) was 96% ± 7%
197 of the value predicted by Faraday’s law (0.5 mM). Unoxidized Fe(II) (before settling) and unsettled Fe
198 (after settling) were <1.2% and <4.7% of the total Fe dosed, respectively. Because the formation of
199 calcite, magnesite or hydroxyapatite in our experiments was limited if not negligible (see Supporting
200 Information), Ca/Mg/P removal measured by ICP-OES was used as a proxy for Ca/Mg/P uptake by EC
201 precipitates. Bacteria attenuation was calculated as the difference between log CFU concentrations before
202 Fe-EC and after settling (samples taken from the supernatant, ~ 3 cm below the surface), and therefore
203 accounts for both inactivation and removal via enmeshment in flocs. Bacteria attenuation experiments
204 were generally replicated three or more times, except for 12 experiments conducted in duplicate or less
205 (see Table S2). We report average bacteria attenuations ± one standard deviation across replicates.

206 Finally, to assess the effect of P/Si on the uptake of carboxyl moieties by EC precipitates, we
207 performed citrate removal experiments using Fe-EC in the presence and absence of oxyanions under
208 conditions identical to *E. coli* removal experiments, using 10 mg/L-Al of alum before settling (Table S1).
209 Citrate concentrations were measured as total C with a TOC-V_{CSH} analyzer (Shimadzu).

210

211 **2.4. ζ-potential measurements and bacterial viability tests**

212 In this study, ζ-potential measurements, which are a proxy for surface charge, were used to assess the
213 interaction of major groundwater ions with the surface of EC precipitates or *E. coli* K12 cells. ζ-potential

214 was measured by dynamic light scattering (Malvern Zetasizer Nano-ZS) at 633 nm. In addition,
 215 qualitative assessments of membrane permeabilization, which were used as a proxy for bacteria
 216 inactivation, were performed with the BacLight LIVE-DEAD kit (Invitrogen) used in conjunction with
 217 fluorescent microscopy (Zeiss AxioImager, 63× Plan-Apochromat objective, EndoGFP and mCherry
 218 filters, UC Berkeley CNR Biological Imaging Facility). Sample preparation and data collection
 219 procedures are described in the Supporting Information.

220

221 2.5. Model of Ca/Mg complexation by bacterial cell walls

222 Drawing on previous work (Johnson et al., 2007; Ngwenya et al., 2003), we derived a simple
 223 equilibrium surface complexation model, which included three bivalent cation adsorption sites on
 224 bacterial cell walls: carboxyl groups, protonated and deprotonated phosphate groups. The model predicts
 225 the percentage of bacterial phosphate and carboxyl groups complexed by Ca and Mg as:

$$226 \quad \%P \text{ groups complexed} = \frac{K_{P1,Ca}[Ca^{2+}] + K_{P1,Mg}[Mg^{2+}] + \frac{K_{A2}}{[H^+]}(K_{P2,Ca}[Ca^{2+}] + K_{P2,Mg}[Mg^{2+}])}{\frac{[H^+]}{K_{A1}} + 1 + \frac{K_{A2}}{[H^+]} + K_{P1,Ca}[Ca^{2+}] + K_{P1,Mg}[Mg^{2+}] + \frac{K_{A2}}{[H^+]}(K_{P2,Ca}[Ca^{2+}] + K_{P2,Mg}[Mg^{2+}])} * 100 \quad (1)$$

$$227 \quad \%C \text{ groups complexed} = \frac{K_{C,Ca}[Ca^{2+}] + K_{C,Mg}[Mg^{2+}]}{\frac{[H^+]}{K_A} + 1 + K_{C,Ca}[Ca^{2+}] + K_{C,Mg}[Mg^{2+}]} * 100 \quad (2)$$

228 Deprotonation constants of bacterial surface functional groups and Ca adsorption constants were
 229 obtained directly from the literature (Johnson et al., 2007). Mg adsorption constants were derived from a
 230 relationship between metal-acetate and metal-bacteria complexation constants proposed by Johnson *et al*
 231 (Johnson et al., 2007). Additional details regarding the derivation of this model, including equilibrium
 232 constants, are given in the Supporting Information and Table S3.

233

234 3. Results and Discussion

235 3.1. Effect of HCO₃⁻ on the contributions of removal and inactivation

236 The effect of 8 mM HCO_3^- on *E. coli* attenuation by Fe-EC and FeCl_3 coagulation is shown in
237 Figure 1a. Representative images of live-dead stained *E. coli* are presented in Figure 1b-e. Whereas 8 mM
238 HCO_3^- did not significantly affect *E. coli* attenuation by coagulation with FeCl_3 , the presence of HCO_3^-
239 decreased attenuation by Fe-EC by ~ 1.2 log. Because no reactive oxidants are produced from an Fe(III)
240 salt (Hug and Leupin, 2003), minimal inactivation occurs during FeCl_3 coagulation (consistent with live-
241 dead staining, Figure 1b-c), which implies that attenuation via FeCl_3 addition is exclusively due to
242 physical removal (enmeshment in flocs). Any difference in precipitate-bacteria adhesion between Fe-EC
243 and FeCl_3 coagulation would lead to higher removal in the latter, because the precipitates generated by
244 FeCl_3 coagulation in a HCO_3^- electrolyte are less crystalline and thus have a higher surface area than Fe-
245 EC precipitates (Schwertmann and Cornell, 2000; van Genuchten et al., 2014b; Voegelin et al., 2010).
246 Consequently, the difference in attenuations between Fe-EC and FeCl_3 coagulation can conservatively be
247 attributed to inactivation.

248 As shown in Figure 1a, HCO_3^- did not affect physical removal, which is consistent with ζ -potential
249 measurements showing that HCO_3^- does not significantly interact with the surface of *E. coli* cells or
250 Fe(III) precipitates (Figure S1). By contrast, 8 mM HCO_3^- decreased inactivation substantially by ~ 1.2
251 log. We found a strong correlation between bacteria inactivation in Fe-EC (Figure 1a) and membrane
252 permeabilization (Figure 1d-e). Membrane damage may be caused by reactive intermediates such as $\text{O}_2^{\bullet-}$,
253 H_2O_2 , and Fe(IV), which are generated during Fenton-type reactions (Hug and Leupin, 2003; Keenan and
254 Sedlak, 2008) and have been associated with bactericidal effects (Alt et al., 1999; Ikawa et al., 2010; Kim
255 et al., 2010). The inhibition of inactivation by HCO_3^- might be explained by the formation of $\text{CO}_3^{\bullet-}$
256 radicals, which are produced when HCO_3^- or Fe(II)-carbonate complexes react with H_2O_2 (Hug and
257 Leupin, 2003; Medinas et al., 2007). $\text{CO}_3^{\bullet-}$ is much more reactive than $\text{O}_2^{\bullet-}$, H_2O_2 , and Fe(IV) (Augusto
258 and Miyamoto, 2011; Jacobsen et al., 1998; Neta et al., 1988) (see Supporting Information), and is
259 therefore a much shorter-lived and less selective oxidant. Thus, we speculate that large HCO_3^-
260 concentrations reduce membrane damage and inactivation by shifting the nature of reactive species

261 produced during Fe-EC towards a shorter-lived oxidant ($\text{CO}_3^{\bullet-}$) that is more likely to die off in the bulk
262 (e.g. reacting with Fe(II), Cl^- , HCO_3^-) than to interact with cell membranes.

263 Overall, Figure 1 shows that both inactivation and removal (via enmeshment in flocs) contribute to
264 *E. coli* attenuation in Fe-EC, and that the concentration of HCO_3^- governs the amount of inactivation. In
265 the remaining sections of our study, we will focus on removal. Interactions between EC precipitates and
266 *E. coli* cells are investigated by varying levels of ionic strength, Ca, Mg, P, and Si. Because these ions are
267 not expected to react with oxidants such as $\text{O}_2^{\bullet-}$, H_2O_2 , or Fe(IV) (Hug and Leupin, 2003; Li et al., 2012;
268 Roberts et al., 2004), nor to interact with lipid aliphatic chains, which are the target of oxidants on cell
269 membranes (lipid peroxidation), they are assumed to have a negligible effect on inactivation. Therefore,
270 their potential impact on *E. coli* attenuation will be solely attributed to changes in removal.

271

272 **3.2. Effect of ionic strength**

273 Increasing ionic strength over 2 orders of magnitude (2-200 mM), which results in increased charge
274 screening (Debye length decreased tenfold), did not significantly affect *E. coli* attenuation by Fe-EC,
275 regardless of the initial electrolyte composition (Figure S2). The negligible effect of ionic strength
276 suggests that electrostatic interactions play a secondary role compared to specific interactions in the
277 adhesion of EC precipitates to *E. coli* cells. In the following two sections, we investigate the bacterial
278 surface sites involved in these interactions by systematically varying the concentration of bivalent cations
279 and oxyanions in order to selectively complex adsorption sites on the surface of *E. coli* cells and EC
280 precipitates, respectively.

281

282 **3.3. Effect of bivalent cations: Ca and Mg**

283 **3.3.1. Single solute electrolytes (no oxyanions, no HCO_3^-)**

284 *E. coli* attenuation as a function of Ca and Mg concentrations is shown in Figure 2a. Ca and Mg both
285 decreased *E. coli* attenuation, with a larger inhibitory effect observed for Mg (2.1 log decrease in

286 attenuation when Mg increased from 0 to 10.6 mM) than for Ca (1.3 log decrease in attenuation when Ca
287 increased from 0 to 12.9 mM). Because bivalent cations should not affect inactivation (see 3.1.), these
288 reductions in bacteria attenuation can be interpreted as reductions in *E. coli* removal.

289 Figure 2b shows the ζ -potential of EC precipitates and *E. coli* cells as a function of Ca/Mg
290 concentrations. In this single Ca/Mg solute electrolyte, EC precipitates were positively charged.
291 Increasing concentrations of Ca/Mg had a limited effect on the ζ -potential of precipitates, suggesting that
292 bivalent cations interacted minimally with their surface. This result was expected given the repulsive
293 electrostatic forces between bivalent cations and positively-charged EC precipitates, and is consistent
294 with previous work showing negligible uptake of Ca/Mg by Fe(III) (oxyhydr)oxides at circumneutral pH
295 in the absence of oxyanions (Kanematsu et al., 2013; Stachowicz et al., 2008). By contrast, Ca and Mg
296 caused a significant increase in the ζ -potential of *E. coli* cells, indicating a strong interaction between
297 bivalent cations and bacteria surfaces. Figure S3 shows the percentage of bacterial functional groups
298 complexed by bivalent cations, as predicted by our equilibrium surface model. According to this model,
299 raising Ca/Mg concentrations from 0 to 13 mM leads to a significant increase in the complexation of
300 carboxyl (from 0 to 70-80%) and phosphate (from 0 to 90-95%) groups, which is consistent with the
301 observed increase in *E. coli* ζ -potential (Figure 2b).

302 Figure 2c combines *E. coli* attenuation results (Figure 2a) and model outputs (Figure S3) to highlight
303 that *E. coli* removal decreases as the percentage of complexed bacterial carboxyl and phosphate groups
304 increases. Stronger inhibition of *E. coli* removal by Mg than by Ca (Figure 2a) is consistent with this
305 trend, because Mg has a higher affinity for bacterial surface functional groups (Beveridge and Koval,
306 1981) (Table S3 and Figure S3).

307 3.3.2. Groundwater-like electrolytes (with oxyanions and HCO_3^-)

308 Figure 2d shows the effect of Ca (0-13.5 mM) and Mg (2.4-10.5 mM) on *E. coli* attenuation in a
309 groundwater-like electrolyte containing 8 mM HCO_3^- , 1.2 mM Si, and 0.4 mM P. Similar to the single

310 Ca/Mg solute system, bivalent cations reduced *E. coli* attenuation, with Ca/Mg concentrations above 10
311 mM leading to a 1-2 log decrease in attenuation.

312 Figure 2e shows ζ -potentials of EC precipitates and *E. coli* cells as a function of Ca/Mg
313 concentrations in the groundwater-like electrolyte. Bivalent cations increased the ζ -potential of *E. coli*
314 cells, consistent with the complexation of phosphate and carboxyl groups on cell walls, as explained in
315 section 3.3.1. In this electrolyte, EC precipitates were negatively-charged due to the sorption of P and, to
316 a lesser extent, Si (P:Fe and Si:Fe molar solids ratios of 0.7 ± 0.1 and 0.06 ± 0.04 , respectively)
317 (Appenzeller et al., 2002; Hamid et al., 2011). In contrast to previous experiments in the absence of
318 oxyanions, bivalent cations significantly interacted with the surface of EC precipitates in the
319 groundwater-like electrolyte, as indicated by a substantially higher ζ -potential at larger Ca/Mg
320 concentrations. This increase in precipitate surface charge coincided with increased Ca/Mg uptake, with
321 solids ratios going from 0.5 ± 0.1 to 1.2 ± 0.7 mol Ca:mol Fe, and from 0.3 ± 0.1 to 0.5 ± 0.4 mol Mg:mol
322 Fe, respectively. EC precipitates with similar chemical compositions (i.e. Ca/Mg:P:Fe molar ratios) have
323 been documented in previous studies performed in nearly identical electrolytes, but in the absence of
324 bacteria (van Genuchten et al., 2014a, 2014b). In these studies, Ca was shown to interact with P sorbed to
325 Fe(III) precipitates, via direct Ca-O-P bonds, and to a lesser extent, electrostatically. In the present study,
326 the observed increase in precipitate ζ -potential with Ca/Mg in the groundwater-like electrolyte is
327 consistent with such interactions of Ca/Mg with P sorbed to EC precipitates.

328 Figure 2f illustrates the inverse relationship between *E. coli* attenuation in the groundwater-like
329 electrolyte and the percentage of bacterial functional groups complexed by Ca/Mg (derived from our
330 model). Figure 2f also includes data from our previous study of *E. coli* attenuation in SBGW containing
331 2.6 mM Ca and 1.9 mM Mg (Delaire et al., 2015), which are consistent with this trend. Finally, we note
332 that *E. coli* attenuations in groundwater-like electrolytes (Figure 2f) were overall ~ 1 log lower than in
333 single solute systems (Figure 2c), which is consistent with the inhibition of inactivation by 8 mM HCO_3^-
334 shown in section 3.1.

335 Taken together, Figures 2a-f show that Ca/Mg decreases *E. coli* removal independent of the
336 electrolyte, and more specifically, independent of the surface charge of EC precipitates: whether Ca/Mg
337 increase (Figure 2b, no oxyanions) or decrease (Figure 2e, oxyanions present) the electrostatic barrier to
338 precipitate adhesion on cell walls, bivalent cations equally inhibit *E. coli* removal. Combined with the
339 limited impact of ionic strength (Section 3.2 and Figure S2), this result confirms the minimal role of
340 electrostatic interactions on *E. coli* removal and instead points to the importance of specific interactions
341 between EC precipitates and bacterial phosphate and/or carboxyl groups. These findings are in good
342 agreement with previous ATR-FTIR studies that provided evidence for direct bonding between Fe oxides
343 and bacterial phosphate/carboxyl groups in more simple and controlled systems (Elzinga et al., 2012;
344 Parikh and Chorover, 2006; Parikh et al., 2014).

345

346 **3.4. Effect of oxyanions: P and Si**

347 **3.4.1. Single solute electrolytes (no bivalent cations, no HCO_3^-)**

348 Figure 3a shows the effect of 0.4 mM Si/P on *E. coli* attenuation in electrolytes containing no Ca/Mg.
349 Whereas Si had no detectable effect, P reduced *E. coli* attenuation by 1.6 log. Because Si and P should not
350 affect inactivation, as explained in section 3.1, these effects correspond to changes in removal via
351 enmeshment in flocs. ζ -potential measurements of EC precipitates and *E. coli* cells as a function of P/Si
352 concentrations are presented in Figure 3b. Si and P had no detectable effect on the ζ -potential of *E. coli*
353 cells, reflecting the absence of interaction between these oxyanions and bacterial cell walls. By contrast,
354 Si and P significantly decreased the ζ -potential of EC precipitates, indicating oxyanion sorption
355 (Appenzeller et al., 2002; Hamid et al., 2011), which is supported by the uptake of Si and P measured by
356 ICP-OES (Si:Fe and P:Fe molar solids ratios of 0.3 and 0.6, respectively). Because electrostatic
357 interactions do not play a major role in *E. coli* removal, as demonstrated above, lower bacteria removal in
358 the presence of P cannot be explained by the decrease in precipitate surface charge. Rather, the results in
359 Figure 3a indicate that inorganic aqueous P competes with bacterial functional groups involved in

360 bonding to EC precipitates. By contrast, our results indicate that Si does not strongly compete with these
361 functional groups.

362 Because aqueous P and bacterial phosphate groups are structurally and chemically similar, they are
363 expected to compete for precipitate surfaces. However, the competition between P and carboxyl groups is
364 less straight-forward. To assess the effect of P on the adsorption of carboxyl moieties, we measured the
365 removal of citrate (a proxy for carboxyl groups) by Fe-EC in the presence and absence of P. As shown in
366 Figure 3c, P decreased citrate removal by nearly 54% (initial P:C molar ratio of 0.9). In *E. coli* attenuation
367 experiments, the molar ratio of aqueous P to bacterial surface carboxyl groups is ~ 2500 mol P: mol C
368 (see Supporting Information). Therefore, aqueous P is expected to strongly compete with bacterial
369 carboxyl groups in attenuation experiments.

370 Fe(III) (oxyhydr)oxides have a much higher affinity for P than for Si (Li et al., 2014; Roberts et al.,
371 2004). Therefore, Si is not expected to effectively compete with bacterial phosphate groups for precipitate
372 surfaces. However, Figure 3c shows that Si decreased citrate removal in Fe-EC by nearly 20% (initial
373 Si:C molar ratio of 0.7). In *E. coli* attenuation experiments, where the molar ratio of Si to bacterial surface
374 carboxyl groups is orders of magnitude higher (~ 2500, see Supporting Information), it is thus likely that
375 Si would inhibit bacteria removal if carboxyl groups played an important role in the adhesion of EC
376 precipitates. Because Si had no detectable effect on *E. coli* attenuation (Figure 3a), we propose that
377 phosphate groups are the primary sites for the adhesion of EC precipitates to cell walls, with negligible
378 contributions from carboxyl groups.

379 **3.4.2. Groundwater-like electrolytes (with bivalent cations, HCO_3^- and Si)**

380 In Figure 3d, we show the effect of P (0-0.4 mM) on *E. coli* attenuation in the presence of Ca (2 and 9
381 mM) or Mg (8 mM) in a groundwater-like electrolyte containing 8 mM HCO_3^- and 1.2 mM Si. In contrast
382 to experiments in electrolytes free of bivalent cations, where P decreased *E. coli* removal by 1.6 log
383 (Figure 3a), 0.4 mM P had no effect on *E. coli* removal in the presence of Ca/Mg. We note that lower *E.*

384 *coli* attenuations in Figure 3d compared to Figure 3a (~ - 2 log) are due to the inhibition of inactivation by
385 8 mM HCO₃⁻ (shown in section 3.1) and to the reduction in removal caused by Ca/Mg (shown in section
386 3.3).

387 Figures 3e-f show ζ-potential measurements of EC precipitates and *E. coli* cells, respectively, as a
388 function of P concentration in the groundwater-like electrolyte containing bivalent cations. Figure 3e
389 shows that P did not interact significantly with bacterial cells, as expected. In contrast to single oxyanion
390 systems (Figure 3b), EC precipitates in the groundwater-like electrolyte were negatively-charged for all P
391 concentrations, due to sorbed Si/P. In addition, the ζ-potential of EC precipitates did not decrease when
392 the P concentration increased from 0 to 0.4 mM, despite substantial P uptake by precipitates (P:Fe molar
393 solids ratios of 0.6-0.8, see Table S4). This result stands in strong contrast with electrolytes containing no
394 Ca/Mg, where high concentrations of P (0.4 mM) and similar P:Fe solids ratios (0.6 mol:mol)
395 significantly decreased EC precipitate surface charge (Figure 3b). In the groundwater-like electrolytes,
396 ICP-OES measurements indicated that Ca/Mg uptake by EC precipitates increased by 20-200% –
397 depending on the initial Ca/Mg concentration– in the presence of 0.4 mM P (Table S4). This co-sorption
398 of Ca/Mg explains the negligible impact of P sorption on the surface charge of EC precipitates.

399 Based on the co-sorption of Ca/Mg and P, the behavior of precipitate and bacteria surfaces, and the
400 negligible effect of P on *E. coli* removal observed in our system, we propose that Ca/Mg can act as a
401 bivalent cation bridge between bacterial phosphate groups and P sorbed to EC precipitates. This Ca/Mg
402 configuration, which creates additional sites at the precipitate surface that can interact with bacterial cell
403 walls, is consistent with the Ca-P-Fe configurations documented previously in comparable systems (Senn
404 et al., 2015; van Genuchten et al., 2014a; Voegelin et al., 2010).

405

406 **3.5. Attenuation of different types of bacteria**

407 The attenuation of *E. coli* K12, *E. coli* ECOR 10 and *E. faecalis* in SBGW with an Fe dosage of 0.5
408 mM is shown in Figure 4. No significant difference between the log attenuations of the three different
409 bacterial strains was observed, despite their considerably different cell wall structures. For example, the
410 surface of Gram-positive *E. faecalis* is composed of a peptidoglycan layer topped with teichoic acids,
411 whereas the surface of Gram-negative *E. coli* is made of phospholipids and lipopolysaccharides (LPS)
412 (Madigan et al., 2000). Furthermore, the two *E. coli* strains differ by the length of their LPS: ECOR 10 is
413 a smooth strain with a full-length LPS (with O-antigen), whereas K12 is a rough strain with a truncated
414 LPS (no O-antigen). Such differences in cell wall composition lead to differences in hydrophobicity,
415 surface charge, surface roughness and steric hindrance to approach mineral surfaces and nanoparticles
416 (Chen and Walker, 2012; Jacobson et al., 2015; Walker et al., 2004).

417 Previous studies have found that cell wall composition and LPS length affect the interactions of
418 bacteria with mineral surfaces (sand, iron-oxide coated sand, and gold nanoparticles) in systems governed
419 by non-specific interactions, such as electrostatic, steric, hydrophobic, and van der Waals forces (Chen
420 and Walker, 2012; Jacobson et al., 2015; Mohanty et al., 2013; Truesdail et al., 1998; Walker et al.,
421 2004). In contrast to these studies, similar attenuation of *E. coli* K12, *E. coli* ECOR 10 and *E. faecalis* in
422 our system is likely due to the dominant role of specific interactions in bacteria-precipitate adhesion.
423 Phosphate functional groups, which we showed are the primary binding sites for EC precipitates, are
424 present in similar abundance on Gram-negative and Gram-positive bacteria (Borrok et al., 2005) (mainly
425 on phospholipids and on teichoic acids, respectively), explaining similar removal of *E. coli* and *E. faecalis*.
426 In addition, negligible steric hindrance from longer LPS on *E. coli* is likely due to the small size of EC
427 precipitates compared to bacterial cells (Figure S4).

428 Based on these results, we expect that Fe-EC would be similarly effective for all waterborne
429 pathogenic bacteria, both Gram-negative (e.g. *Vibrio cholera*, *Shigella*, *Salmonella*, pathogenic *E. coli*)
430 and Gram-positive (e.g. *E. faecalis*, *Bacillus cereus*, *Staphylococcus aureus*). Finally, similar attenuation
431 of *E. coli* K12 and *E. coli* ECOR 10 suggests that fecal pathogens, which are typically smooth strains

432 (Felix and Pitt, 1935), would be as effectively removed as our model indicator *E. coli* K12. Overall, these
433 results are promising for the application of Fe-EC to drinking water or wastewater treatment.

434

435 **4. Conclusions**

436 In this study, we showed that bacteria inactivation, which can be significant in the absence of oxidant
437 scavengers, is largely suppressed by HCO_3^- concentrations characteristic of natural waters. Therefore, we
438 expect physical removal to be the primary process of bacteria attenuation in most water treatment
439 applications. Sludge sterilization before handling and disposal (e.g. via heat treatment) may therefore be
440 necessary as flocs may contain viable pathogens.

441 We have shown that removal is driven by the interactions of EC precipitates with bacterial phosphate
442 groups, which may bind to Fe(III) surfaces directly or via a Ca/Mg bridge to P sorbed on precipitates. In
443 light of these mechanisms, the contrasted effects of P and Si observed in this study can be generalized to
444 other strongly- (e.g., arsenate) and weakly- (e.g., borate, arsenite, nitrate) sorbing oxyanions, respectively.
445 Similarly, the observed impact of Ca/Mg (hardness) can be extrapolated to metallic bivalent cations that
446 may be present in wastewater, such as Cu^{2+} , Cd^{2+} , Pb^{2+} , and Zn^{2+} .

447 Consistent with the universal presence of phosphate groups on bacteria surfaces, Fe-EC is equally
448 effective towards Gram-positive and Gram-negative bacteria, rough and smooth alike. Our results
449 strongly suggest that Fe-EC, which is a technology applicable to decentralized arsenic remediation in
450 low-resource settings (Amrose et al., 2014; Holt et al., 2005), can also effectively remove all types of
451 bacterial contamination from a wide range of groundwater sources. Field validation of these promising
452 results as well as an investigation of virus attenuation are needed to confirm the potential of Fe-EC to
453 substitute for existing disinfection methods when applied to groundwater treatment.

454

455 **Acknowledgements**

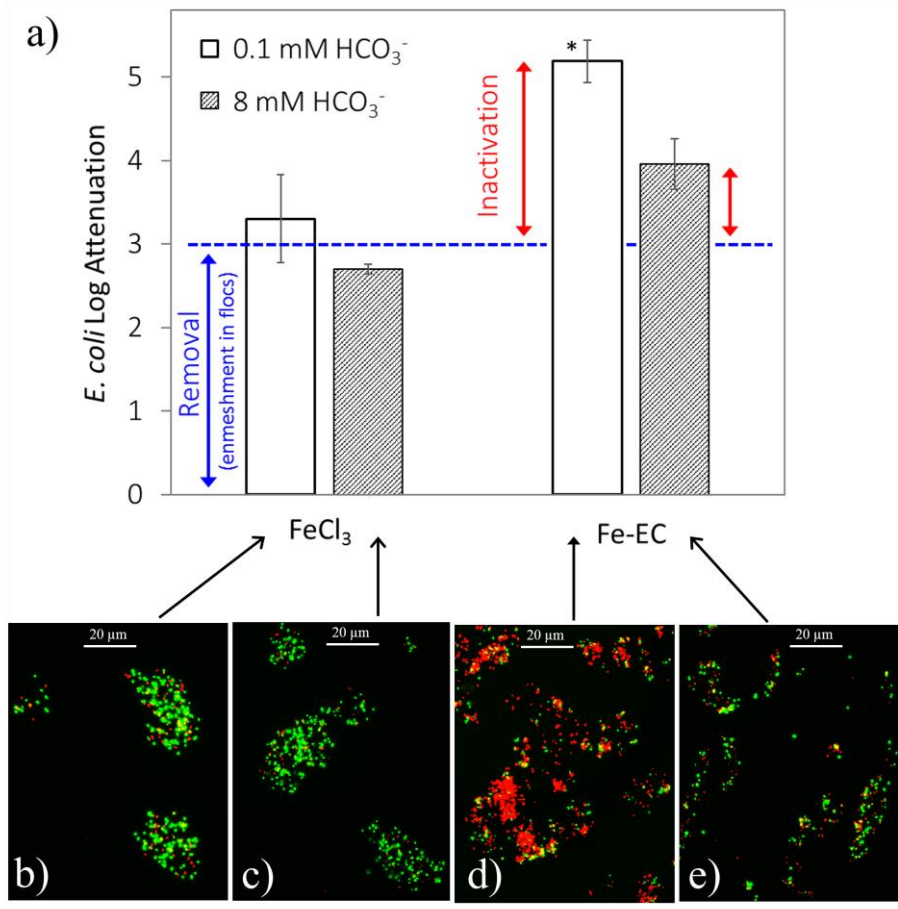
456 This work was supported by the Development Impact Lab (USAID Cooperative Agreement AID-OAA-
457 A-13-00002) and the Andrew and Virginia Rudd Family Foundation Chair for Safe Water and Sanitation
458 administered by the Blum Center for Developing Economies. Additionally, C.M.v.G. acknowledges
459 funding support from the Netherlands Organization for Scientific Research (NWO) through a Veni grant.
460 We wish to express our gratitude to Kara Nelson, who provided useful discussions regarding the
461 complexation of Ca/Mg to bacterial functional groups, and to David Sedlak, Denise Schichnes, John
462 Wertz and Aidan Cecchetti for their kind assistance along various steps of this work. ζ -potential
463 measurements were conducted at the Molecular Foundry of Lawrence Berkeley National Laboratory and
464 supported by the Office of Science, Office of Basic Energy Sciences, of the U.S. Department of Energy
465 under Contract No. DE-AC02-05CH11231.

466

467 **Supporting Information**

468 The Supporting Information provides detailed descriptions of experimental protocols (for Fe-EC
469 experiments, ζ -potential measurements, and fluorescent microscopy), the bacteria surface complexation
470 model, and the reactivity of strong oxidants produced in Fe-EC. Supporting figures and tables referenced
471 in the text are also included.

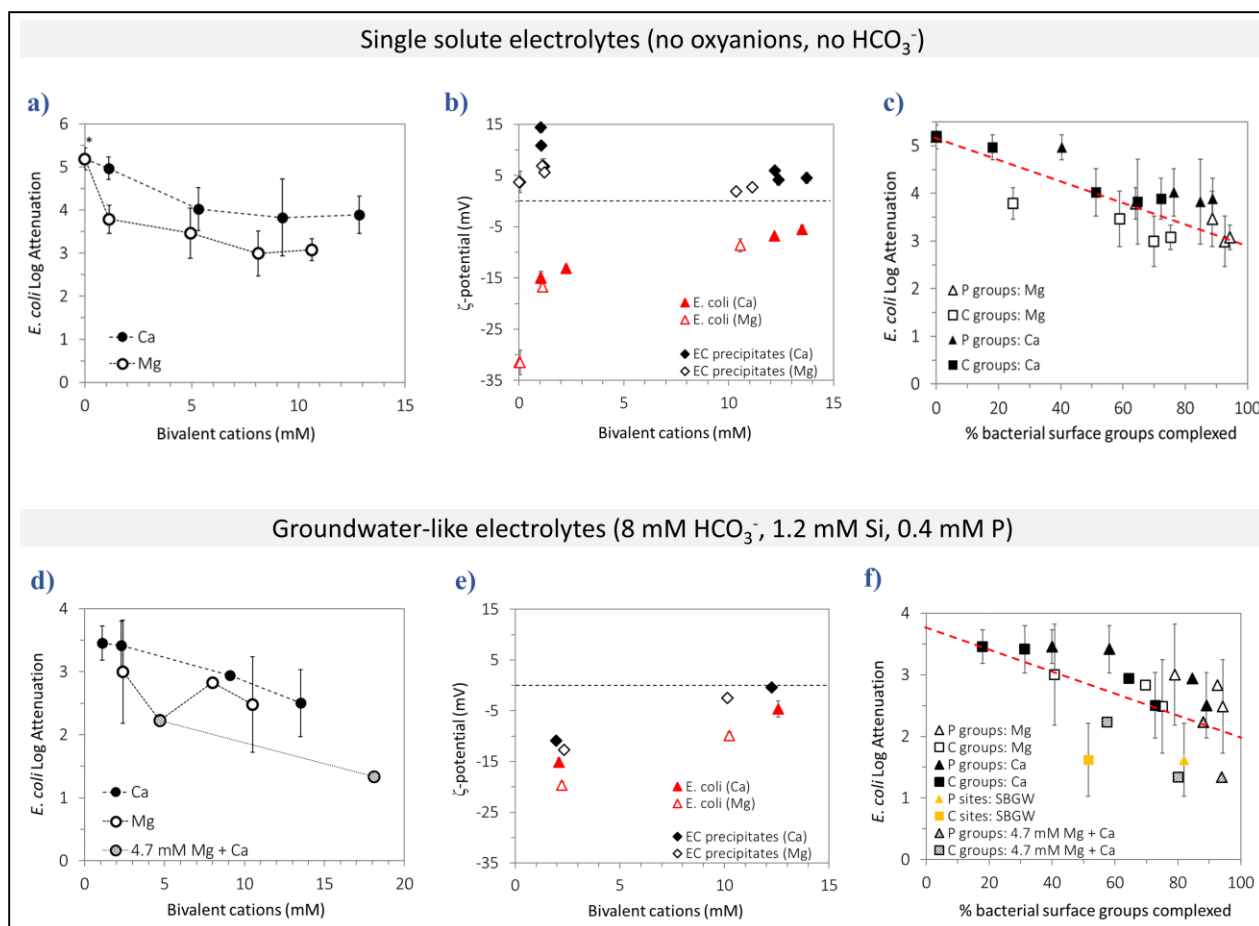
472



473

474 **Figure 1: *E. coli* attenuation with Fe-EC and FeCl₃, with and without 8 mM HCO₃⁻.** Fe dosage was
 475 0.5 mM in all experiments. Panel a shows *E. coli* log attenuations. The asterisk indicates that the detection
 476 limit for bacteria attenuation was reached for some of the replicate experiments. Panels b-e show
 477 fluorescent microscopy images of live (green)-dead (red) stained *E. coli* cells. The blue dashed line is the
 478 average attenuation in all FeCl₃ experiments (with and without HCO₃⁻) and represents removal (blue
 479 arrow). *E. coli* log attenuations are compared to this baseline to deduce approximate log inactivations (red
 480 arrows). All experiments were conducted at pH 7.0. In 0.1 mM HCO₃⁻ experiments, 2 mM NaCl were
 481 added for conductivity.

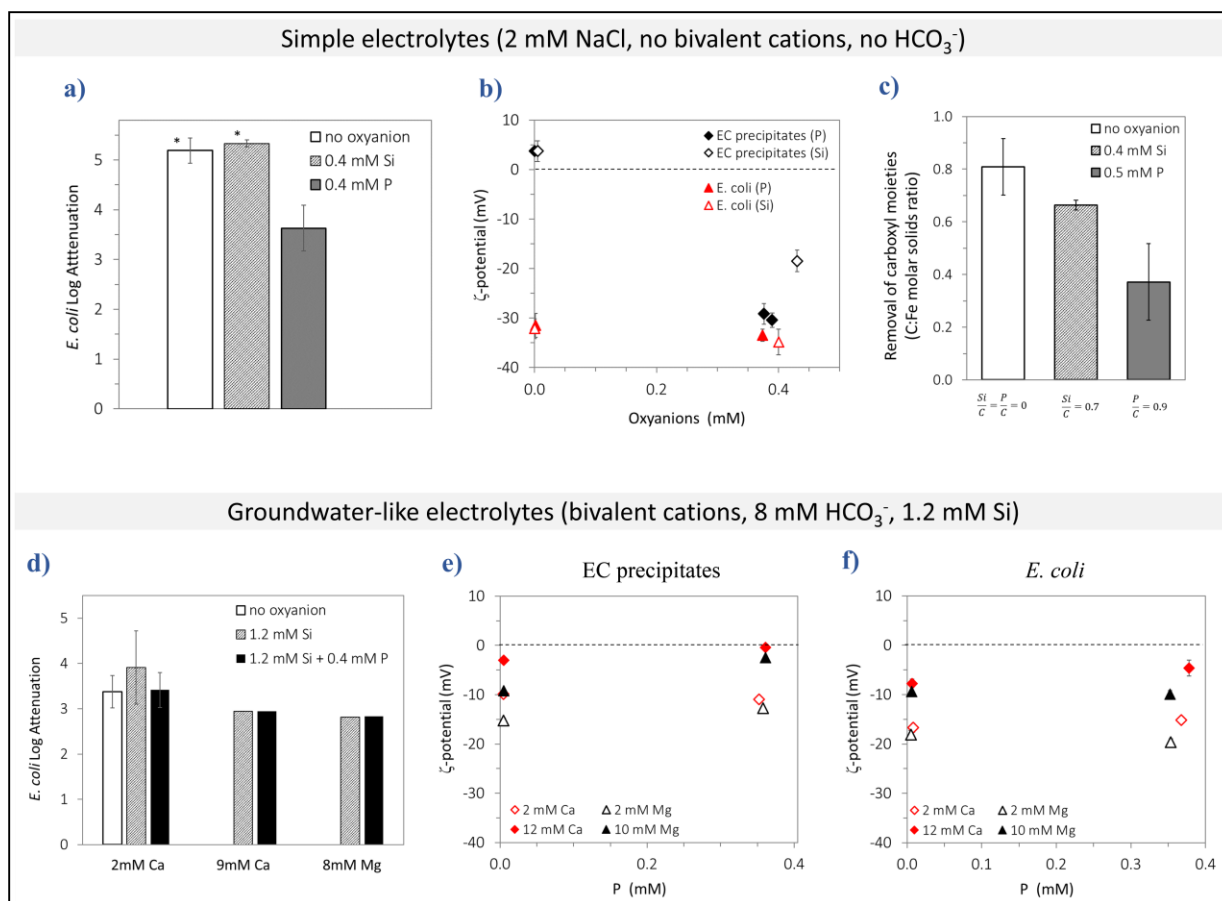
482



483

484 **Figure 2: Effect of Ca and Mg on *E. coli* attenuation in Fe-EC, in single solute electrolytes (panels a, b**
 485 **and c) and in groundwater-like electrolytes containing 8 mM HCO₃⁻, 1.2 mM Si and 0.4 mM P (panels d,**
 486 **e and f). Panels a and d: effect of increasing Ca/Mg concentrations on *E. coli* log attenuation with an Fe**
 487 **dosage of 0.5 mM. The asterisk indicates that the detection limit for bacteria attenuation was reached for**
 488 **some of the replicate experiments. Panels b and e: effect of increasing Ca/Mg concentrations on the ζ -**
 489 **potential of EC precipitates and *E. coli* cells (data points for 0 mM Ca and 0 mM Mg overlap on panel b).**
 490 **Panels c and f: *E. coli* attenuation as a function of complexed bacterial surface groups (combination of**
 491 **Figures 2a and S3, and 2d and S3 respectively). The dotted red lines highlight the inverse correlation**
 492 **between *E. coli* attenuation and the complexation of bacterial functional groups. All experiments were**
 493 **conducted at pH 7.0. Experiments with no Ca/Mg (panel a) were conducted in 2 mM NaCl for**
 494 **conductivity.**

495



496

497 **Figure 3: Effect of P and Si on *E. coli* attenuation by Fe-EC with an Fe dosage of 0.5 mM in single**
 498 **solute electrolytes (0.4 mM P or Si in 2mM NaCl background for conductivity; panels a,b and c) and**
 499 **groundwater-like electrolytes containing 8 mM HCO₃⁻, 1.2 mM Si and bivalent cations (panels, d, e and f).**
 500 **a) Effect of Si and P on *E. coli* attenuation. Asterisks indicate that the detection limit for bacteria**
 501 **attenuation was reached for some of the replicate experiments. b) Effect of Si (open symbols) and P (solid**
 502 **symbols) on the ζ -potential of EC precipitates and *E. coli* cells. c) Effect of P and Si on the removal of**
 503 **citrate (a proxy for carboxyl moieties) by Fe-EC. d) Effect of P on *E. coli* attenuation at different levels of**
 504 **Ca/Mg. e) Effect of P on the ζ -potential of EC precipitates. f) Effect of P on the ζ -potential of *E. coli***
 505 **cells. All experiments were conducted at pH 7.0.**

506

507

508

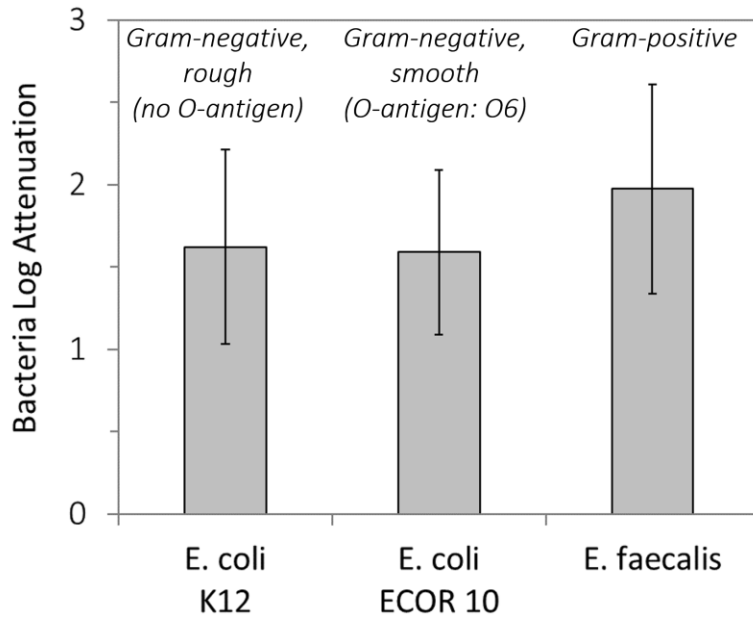
509

510

511

512

513



514

515 **Figure 4: Log attenuation of three different bacterial strains by Fe-EC**, at an Fe dosage of 0.5 mM.
 516 All experiments were conducted at pH 7.5 in SBGW (8.2 mM HCO₃⁻, 2.7 mM Ca, 2.0 mM Mg, 1.3 mM
 517 Si, 0.15 mM P, and 6.3 μM As(III)). The log attenuation of *E. coli* K12 in SBGW shown here has also
 518 been reported elsewhere (Delaire et al., 2015).

519

- 520 Alt, E., Leipold, F., Milatovic, D., Lehmann, G., Heinz, S., Schömig, A., 1999. Hydrogen peroxide for prevention of bacterial
521 growth on polymer biomaterials. *Ann. Thorac. Surg.* 68, 2123–2128. doi:10.1016/S0003-4975(99)00832-2
- 522 Amrose, S.E., Bandaru, S.R.S., Delaire, C., van Genuchten, C.M., Dutta, A., DebSarkar, A., Orr, C., Roy, J., Das, A., Gadgil,
523 A.J., 2014. Electro-chemical arsenic remediation: field trials in West Bengal. *Sci. Total Environ.* 488-489, 539–46.
524 doi:10.1016/j.scitotenv.2013.11.074
- 525 Appenzeller, B.M.R., Duval, Y.B., Thomas, F., Block, J.-C., 2002. Influence of Phosphate on Bacterial Adhesion onto Iron
526 Oxyhydroxide in Drinking Water. *Environ. Sci. Technol.* 36, 646–652. doi:10.1021/es010155m
- 527 Arai, Y., Sparks, D.L., 2001. ATR–FTIR Spectroscopic Investigation on Phosphate Adsorption Mechanisms at the Ferrihydrite–
528 Water Interface. *J. Colloid Interface Sci.* 241, 317–326. doi:10.1006/jcis.2001.7773
- 529 Augusto, O., Miyamoto, S., 2011. Oxygen Radicals and Related Species | Ohara Augusto - Academia.edu, in: Pantopoulos, H.M.
530 (Ed.), *Principles of Free Radical Biomedicine*. Volume 1. Nova Science Publishers, Inc.
- 531 Barrera-Díaz, C., Ureña-Nuñez, F., Campos, E., Palomar-Pardavé, M., Romero-Romo, M., 2003. A combined electrochemical-
532 irradiation treatment of highly colored and polluted industrial wastewater. *Radiat. Phys. Chem.* 67, 657–663.
533 doi:10.1016/S0969-806X(02)00497-8
- 534 Beveridge, T.J., Koval, S.F., 1981. Binding of metals to cell envelopes of *Escherichia coli* K-12. *Appl. Environ. Microbiol.* 42,
535 325–35.
- 536 Borrok, D., Turner, B.F., Fein, J.B., 2005. A universal surface complexation framework for modeling proton binding onto
537 bacterial surfaces in geologic settings. *Am. J. Sci.* 305, 826–853. doi:10.2475/ajs.305.6-8.826
- 538 Chan, C.S., Fakra, S.C., Edwards, D.C., Emerson, D., Banfield, J.F., 2009. Iron oxyhydroxide mineralization on microbial
539 extracellular polysaccharides. *Geochim. Cosmochim. Acta* 73, 3807–3818.
- 540 Chassé, A.W., Ohno, T., Higgins, S.R., Amirbahman, A., Yildirim, N., Parr, T.B., 2015. Chemical Force Spectroscopy Evidence
541 Supporting the Layer-by-Layer Model of Organic Matter Binding to Iron (oxy)Hydroxide Mineral Surfaces. *Environ. Sci.*
542 *Technol.* 49, 9733–41. doi:10.1021/acs.est.5b01877
- 543 Chen, G., Walker, S.L., 2012. Fecal indicator bacteria transport and deposition in saturated and unsaturated porous media.
544 *Environ. Sci. Technol.* 46, 8782–90. doi:10.1021/es301378q
- 545 Delaire, C., van Genuchten, C.M., Nelson, K.L., Amrose, S.E., Gadgil, A.J., 2015. *Escherichia coli* Attenuation by Fe
546 Electrocoagulation in Synthetic Bengal Groundwater: Effect of pH and Natural Organic Matter. *Environ. Sci. Technol.* 49,
547 9945–53. doi:10.1021/acs.est.5b01696
- 548 Elzinga, E.J., Huang, J.-H., Chorover, J., Kretzschmar, R., 2012. ATR-FTIR spectroscopy study of the influence of pH and
549 contact time on the adhesion of *Shewanella putrefaciens* bacterial cells to the surface of hematite. *Environ. Sci. Technol.*
550 46, 12848–55. doi:10.1021/es303318y
- 551 Felix, A., Pitt, R.M., 1935. Virulence and Immunogenic Activities of *B. typhosus* in Relation to its Antigenic Constituents. *J.*
552 *Hyg. (Lond.)* 35, 428–36.
- 553 Filius, J.D., Lumsdon, D.G., Meeussen, J.C.L., Hiemstra, T., Van Riemsdijk, W.H., 2000. Adsorption of fulvic acid on goethite.
554 *Geochim. Cosmochim. Acta* 64, 51–60. doi:10.1016/S0016-7037(99)00176-3
- 555 Ghernaout, D., Badis, A., Kellil, A., Ghernaout, B., 2008. Application of electrocoagulation in *Escherichia coli* culture and two
556 surface waters. *Desalination* 219, 118–125. doi:10.1016/j.desal.2007.05.010
- 557 Hamid, R.D., Swedlund, P.J., Song, Y., Miskelly, G.M., 2011. Ionic strength effects on silicic acid (H₄SiO₄) sorption and
558 oligomerization on an iron oxide surface: an interesting interplay between electrostatic and chemical forces. *Langmuir* 27,
559 12930–7. doi:10.1021/la201775c
- 560 Holt, P.K., Barton, G.W., Mitchell, C.A., 2005. The future for electrocoagulation as a localised water treatment technology.
561 *Chemosphere* 59, 355–67. doi:10.1016/j.chemosphere.2004.10.023
- 562 Hug, S.J., Leupin, O., 2003. Iron-catalyzed oxidation of arsenic(III) by oxygen and by hydrogen peroxide: pH-dependent
563 formation of oxidants in the Fenton reaction. *Environ. Sci. Technol.* 37, 2734–42.
- 564 Ikawa, S., Kitano, K., Hamaguchi, S., 2010. Effects of pH on Bacterial Inactivation in Aqueous Solutions due to Low-
565 Temperature Atmospheric Pressure Plasma Application. *Plasma Process. Polym.* 7, 33–42. doi:10.1002/ppap.200900090
- 566 Jacobsen, F., Holcman, J., Sehested, K., 1998. Reactions of the ferryl ion with some compounds found in cloud water. *Int. J.*
567 *Chem. Kinet.* 30, 215–221. doi:10.1002/(SICI)1097-4601(1998)30:3<215::AID-KIN7>3.0.CO;2-V

- 568 Jacobson, K.H., Gunsolus, I.L., Kuech, T.R., Troiano, J.M., Melby, E.S., Lohse, S.E., Hu, D., Chrisler, W.B., Murphy, C.J., Orr,
569 G., Geiger, F.M., Haynes, C.L., Pedersen, J.A., 2015. Lipopolysaccharide Density and Structure Govern the Extent and
570 Distance of Nanoparticle Interaction with Actual and Model Bacterial Outer Membranes. *Environ. Sci. Technol.* 49,
571 10642–10650. doi:10.1021/acs.est.5b01841
- 572 Johnson, K.J., Szymanowski, J.E.S., Borrok, D., Huynh, T.Q., Fein, J.B., 2007. Proton and metal adsorption onto bacterial
573 consortia: Stability constants for metal–bacterial surface complexes. *Chem. Geol.* 239, 13–26.
- 574 Kanematsu, M., Young, T.M., Fukushi, K., Green, P.G., Darby, J.L., 2013. Arsenic(III, V) adsorption on a goethite-based
575 adsorbent in the presence of major co-existing ions: Modeling competitive adsorption consistent with spectroscopic and
576 molecular evidence. *Geochim. Cosmochim. Acta* 106, 404–428. doi:10.1016/j.gca.2012.09.055
- 577 Keenan, C.R., Sedlak, D.L., 2008. Factors Affecting the Yield of Oxidants from the Reaction of Nanoparticulate Zero-Valent
578 Iron and Oxygen. *Environ. Sci. Technol.* 42, 1262–1267. doi:10.1021/es7025664
- 579 Kelly, S.D., Hesterberg, D., Ravel, B., 2008. Analysis of soils and minerals using X-ray absorption spectroscopy, in: *Methods of*
580 *Soil Analysis. Part 5. Mineralogical Methods.*
- 581 Kim, J.Y., Park, H.-J., Lee, C., Nelson, K.L., Sedlak, D.L., Yoon, J., 2010. Inactivation of *Escherichia coli* by nanoparticulate
582 zerovalent iron and ferrous ion. *Appl. Environ. Microbiol.* 76, 7668–70. doi:10.1128/AEM.01009-10
- 583 Li, L., Li, J., Shao, C., Zhang, K., Yu, S., Gao, N., Deng, Y., Yin, D., 2014. Arsenic removal in synthetic ground water using iron
584 electrolysis. *Sep. Purif. Technol.* 122, 225–230. doi:10.1016/j.seppur.2013.11.012
- 585 Li, L., van Genuchten, C.M., Addy, S.E.A., Yao, J., Gao, N., Gadgil, A.J., 2012. Modeling As(III) oxidation and removal with
586 iron electrocoagulation in groundwater. *Environ. Sci. Technol.* 46, 12038–45. doi:10.1021/es302456b
- 587 Madigan, M.T., Martinko, J.M., Parker, J., 2000. *Brock biology of microorganisms.* Prentice Hall, Upper Saddle River NJ.
- 588 Mazel, D., Dychinco, B., Webb, V.A., Davies, J., 2000. Antibiotic resistance in the ECOR collection: integrons and identification
589 of a novel aad gene. *Antimicrob. Agents Chemother.* 44, 1568–74.
- 590 McBride, M.B., Kung, K.-H., 1991. Adsorption of phenol and substituted phenols by iron oxides. *Environ. Toxicol. Chem.* 10,
591 441–448. doi:10.1002/etc.5620100403
- 592 Medinas, D.B., Cerchiaro, G., Trindade, D.F., Augusto, O., 2007. The carbonate radical and related oxidants derived from
593 bicarbonate buffer. *IUBMB Life* 59, 255–62. doi:10.1080/15216540701230511
- 594 Miot, J., Benzerara, K., Obst, M., Kappler, A., Hegler, F., Schädler, S., Bouchez, C., Guyot, F., Morin, G., 2009. Extracellular
595 iron biomineralization by photoautotrophic iron-oxidizing bacteria. *Appl. Environ. Microbiol.* 75, 5586–91.
596 doi:10.1128/AEM.00490-09
- 597 Mohanty, S.K., Torkelson, A.A., Dodd, H., Nelson, K.L., Boehm, A.B., 2013. Engineering solutions to improve the removal of
598 fecal indicator bacteria by bioinfiltration systems during intermittent flow of stormwater. *Environ. Sci. Technol.* 47,
599 10791–8. doi:10.1021/es305136b
- 600 Neta, P., Huie, R.E., Ross, A.B., 1988. Rate Constants for Reactions of Inorganic Radicals in Aqueous Solution. *J. Phys. Chem.*
601 *Ref. Data* 17, 1027. doi:10.1063/1.555808
- 602 Ngwenya, B.T., Sutherland, I.W., Kennedy, L., 2003. Comparison of the acid-base behaviour and metal adsorption
603 characteristics of a gram-negative bacterium with other strains. *Appl. Geochemistry* 18, 527–538.
- 604 Norén, K., Loring, J.S., Persson, P., 2008. Adsorption of alpha amino acids at the water/goethite interface. *J. Colloid Interface*
605 *Sci.* 319, 416–28. doi:10.1016/j.jcis.2007.11.046
- 606 Parikh, S.J., Chorover, J., 2006. ATR-FTIR spectroscopy reveals bond formation during bacterial adhesion to iron oxide.
607 *Langmuir* 22, 8492–500. doi:10.1021/la061359p
- 608 Parikh, S.J., Mukome, F.N.D., Zhang, X., 2014. ATR-FTIR spectroscopic evidence for biomolecular phosphorus and carboxyl
609 groups facilitating bacterial adhesion to iron oxides. *Colloids Surf. B. Biointerfaces* 119, 38–46.
610 doi:10.1016/j.colsurfb.2014.04.022
- 611 Roberts, L.C., Hug, S.J., Ruettimann, T., Billah, M.M., Khan, A.W., Rahman, M.T., 2004. Arsenic Removal with Iron(II) and
612 Iron(III) in Waters with High Silicate and Phosphate Concentrations. *Environ. Sci. Technol.* 38, 307–315.
613 doi:10.1021/es0343205
- 614 Schwertmann, U., Cornell, R.M., 2000. *Iron Oxides in the Laboratory: Preparation and Characterization.* Wiley.
- 615 Senn, A.-C., Kaegi, R., Hug, S.J., Hering, J.G., Mangold, S., Voegelin, A., 2015. Composition and structure of Fe(III)-

616 precipitates formed by Fe(II) oxidation in water at near-neutral pH: Interdependent effects of phosphate, silicate and Ca.
617 *Geochim. Cosmochim. Acta* 162, 220–246. doi:10.1016/j.gca.2015.04.032

618 Stachowicz, M., Hiemstra, T., van Riemsdijk, W.H., 2008. Multi-competitive interaction of As(III) and As(V) oxyanions with
619 Ca(2+), Mg(2+), PO(3-)(4), and CO(2-)(3) ions on goethite. *J. Colloid Interface Sci.* 320, 400–14.
620 doi:10.1016/j.jcis.2008.01.007

621 STEC center, 2016. STEC center website [WWW Document]. URL <http://shigatox.net/new/reference-strains/ecor.html> (accessed
622 1.1.16).

623 Stevenson, G., Neal, B., Liu, D., Hobbs, M., Packer, N.H., Batley, M., Redmond, J.W., Lindquist, L., Reeves, P., 1994. Structure
624 of the O antigen of *Escherichia coli* K-12 and the sequence of its rfb gene cluster. *J. Bacteriol.* 176, 4144–56.

625 Truesdail, S., Lukasik, J., Farrah, S., Shah, D., Dickinson, R., 1998. Analysis of Bacterial Deposition on Metal (Hydr)oxide-
626 Coated Sand Filter Media. *J. Colloid Interface Sci.* 203, 369–378. doi:10.1006/jcis.1998.5541

627 van Genuchten, C.M., Addy, S.E.A., Peña, J., Gadgil, A.J., 2012. Removing arsenic from synthetic groundwater with iron
628 electrocoagulation: an Fe and As K-edge EXAFS study. *Environ. Sci. Technol.* 46, 986–94. doi:10.1021/es201913a

629 van Genuchten, C.M., Gadgil, A.J., Peña, J., 2014a. Fe(III) nucleation in the presence of bivalent cations and oxyanions leads to
630 subnanoscale 7 Å polymers. *Environ. Sci. Technol.* 48, 11828–36. doi:10.1021/es503281a

631 van Genuchten, C.M., Peña, J., Amrose, S.E., Gadgil, A.J., 2014b. Structure of Fe(III) precipitates generated by the electrolytic
632 dissolution of Fe(0) in the presence of groundwater ions. *Geochim. Cosmochim. Acta* 127, 285–304.
633 doi:10.1016/j.gca.2013.11.044

634 Voegelin, A., Kaegi, R., Frommer, J., Vantelon, D., Hug, S.J., 2010. Effect of phosphate, silicate, and Ca on Fe(III)-precipitates
635 formed in aerated Fe(II)- and As(III)-containing water studied by X-ray absorption spectroscopy. *Geochim. Cosmochim.*
636 *Acta* 74, 164–186. doi:10.1016/j.gca.2009.09.020

637 Walker, S.L., Redman, J.A., Elimelech, M., 2004. Role of Cell Surface Lipopolysaccharides in *Escherichia coli* K12 adhesion
638 and transport. *Langmuir* 20, 7736–46. doi:10.1021/la049511f

639 WHO, 2011. WHO | Guidelines for drinking-water quality, fourth edition. World Health Organization.

640 Yan, W., Wang, H., Jing, C., 2016. Adhesion of *Shewanella oneidensis* MR-1 to Goethite: A Two-Dimensional Correlation
641 Spectroscopic Study. *Environ. Sci. Technol.* 50, 4343–9. doi:10.1021/acs.est.6b00066

642

643

Figure 1
[Click here to download high resolution image](#)

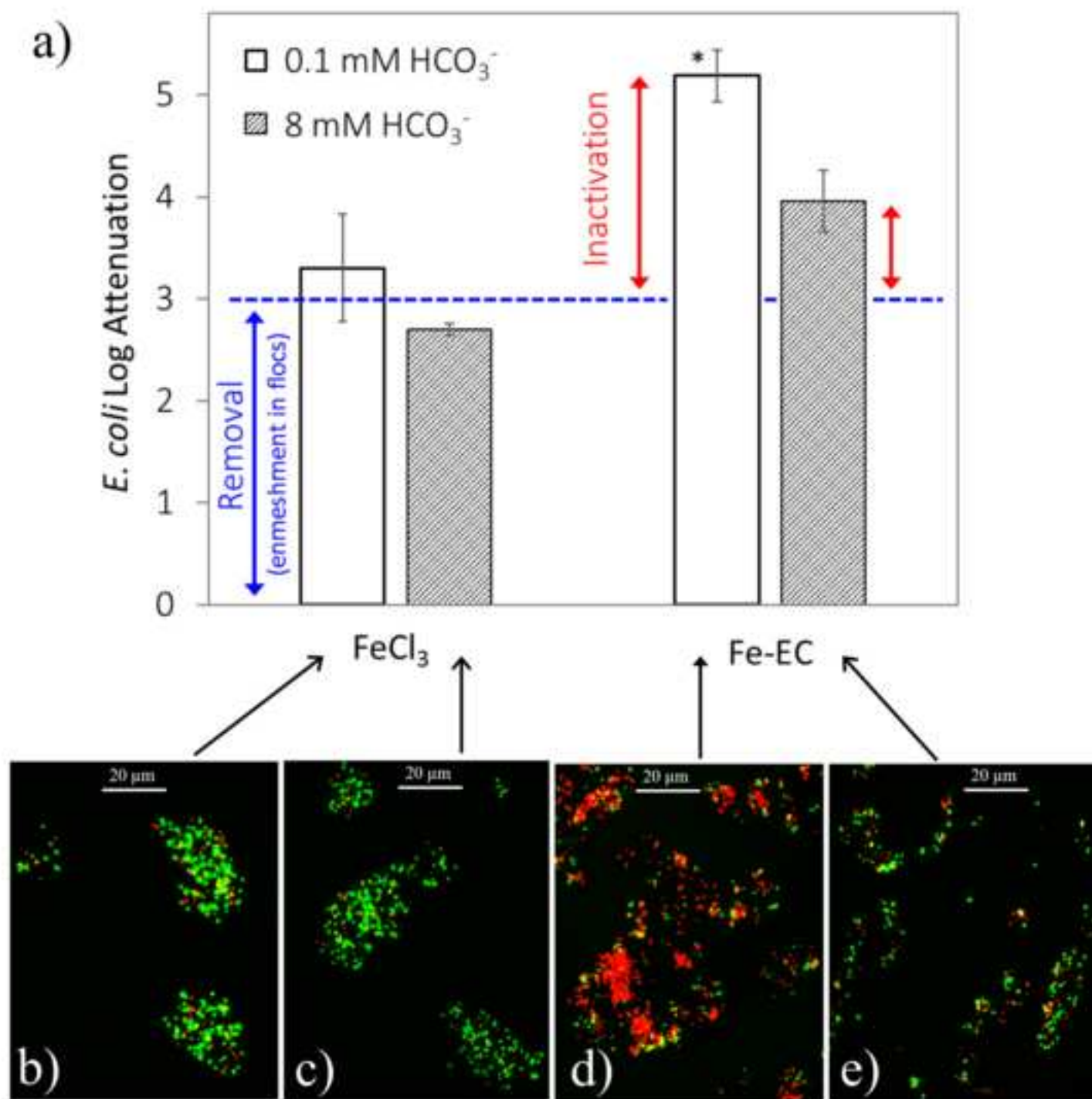
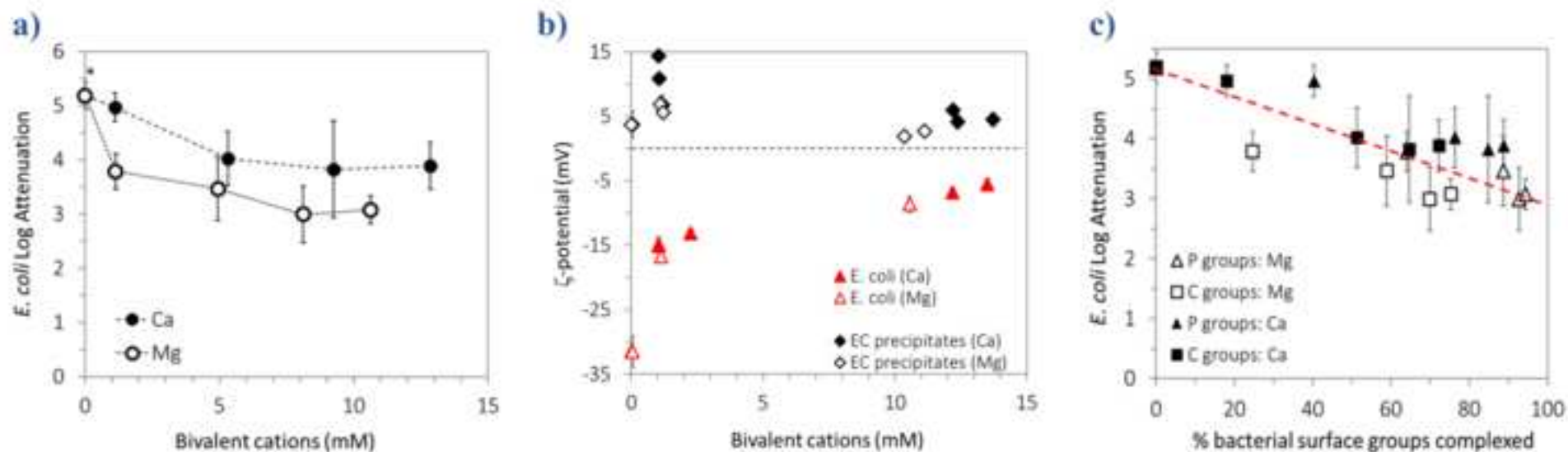


Figure 2
[Click here to download high resolution image](#)

Single solute electrolytes (no oxyanions, no HCO_3^-)



Groundwater-like electrolytes (8 mM HCO_3^- , 1.2 mM Si, 0.4 mM P)

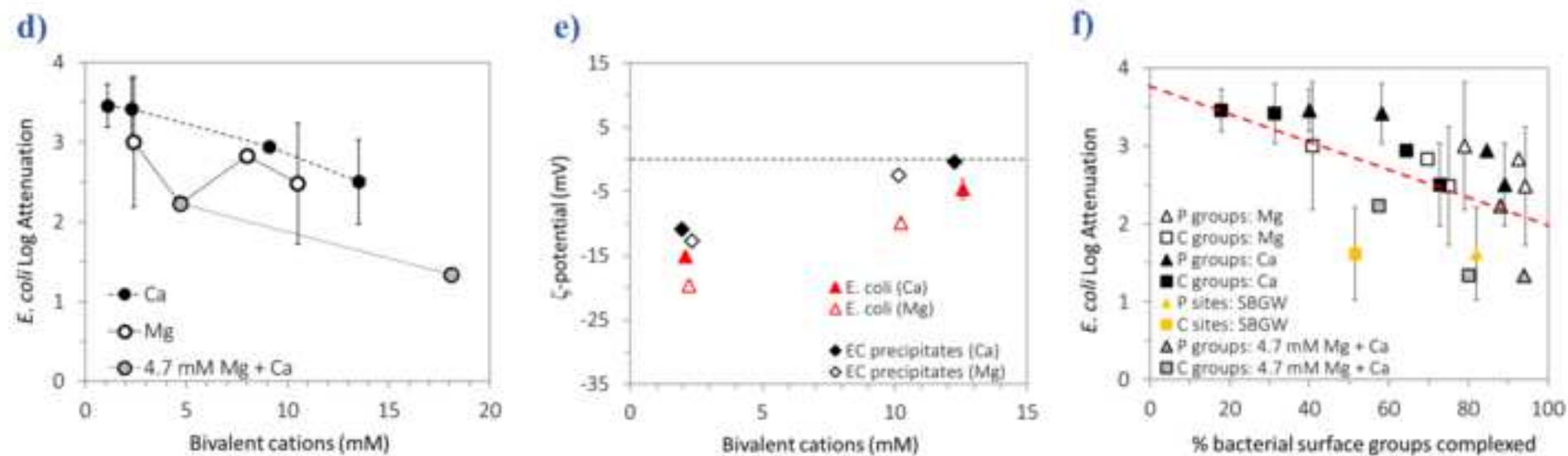
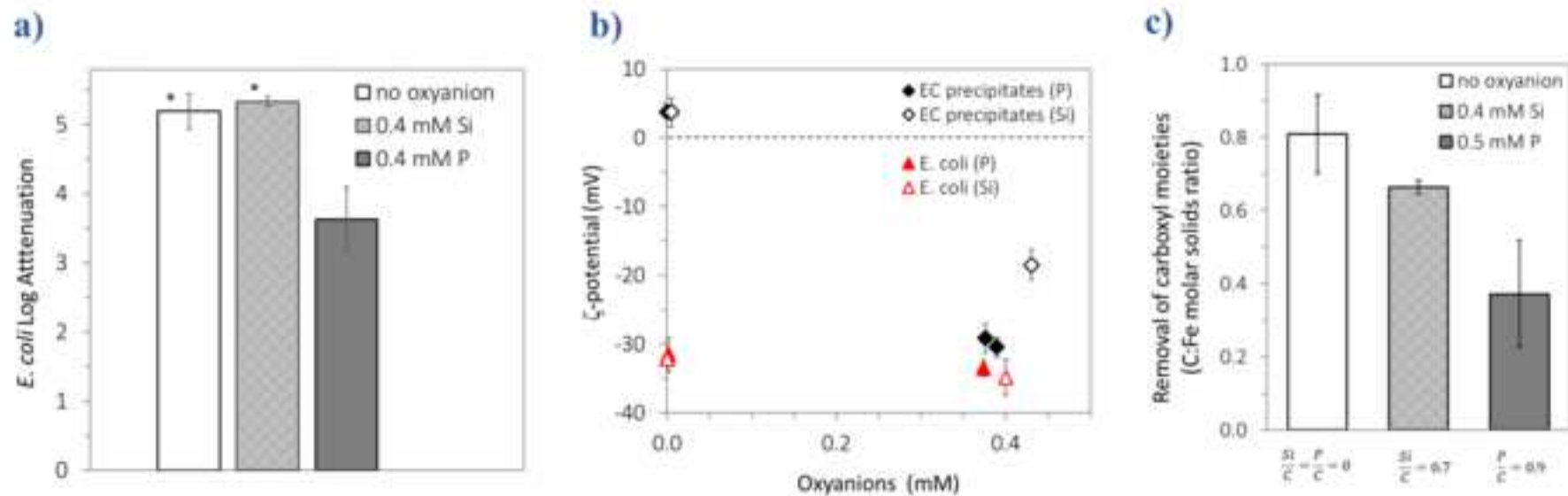


Figure 3
[Click here to download high resolution image](#)

Simple electrolytes (2 mM NaCl, no bivalent cations, no HCO_3^-)



Groundwater-like electrolytes (bivalent cations, 8 mM HCO_3^- , 1.2 mM Si)

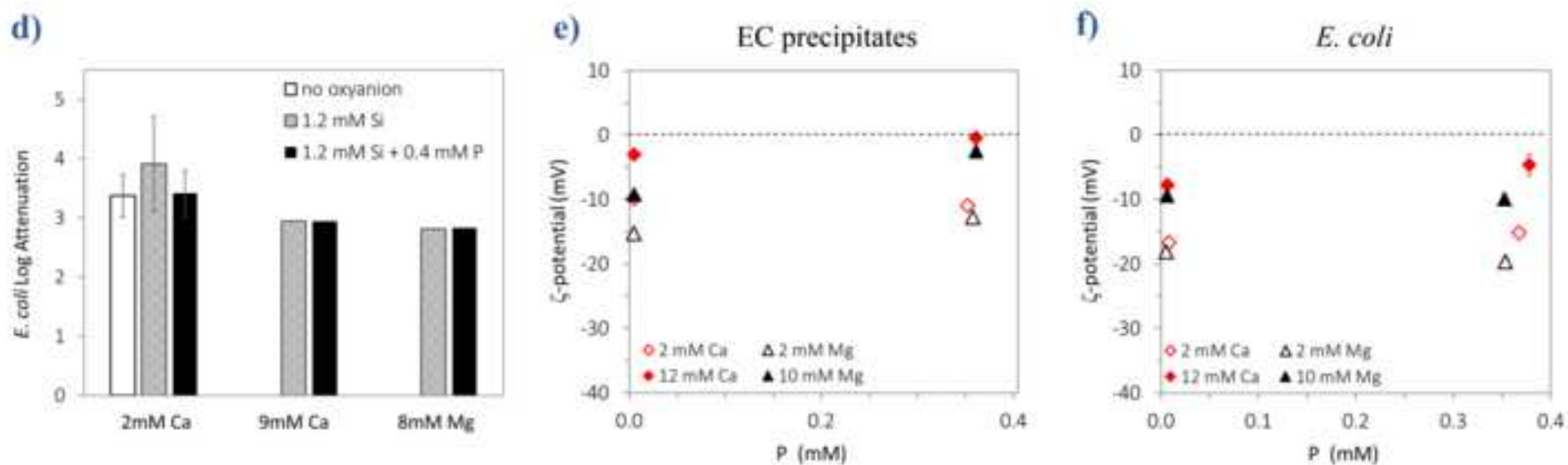
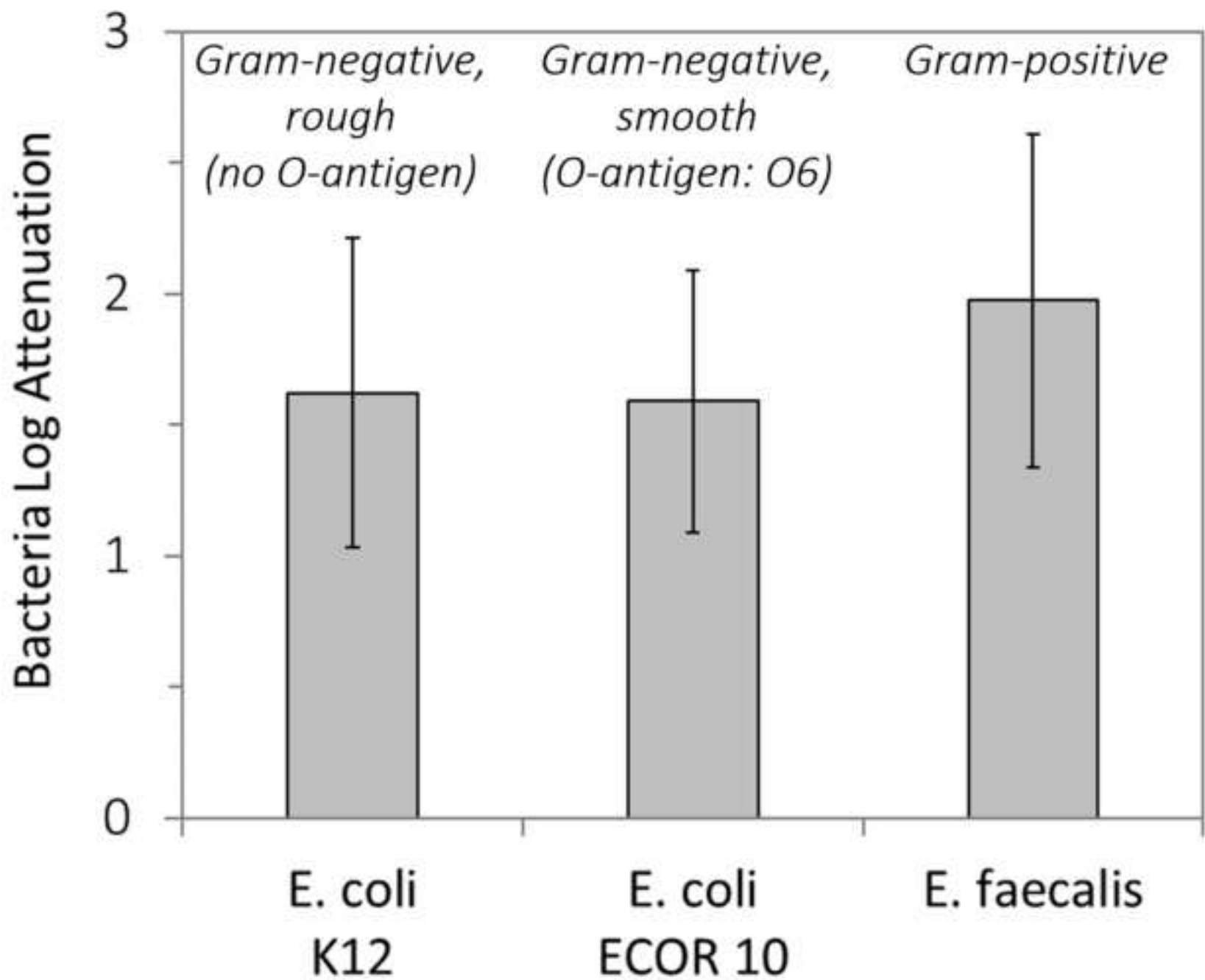


Figure 4
[Click here to download high resolution image](#)



Electronic Supplementary Material (for online publication only)

[Click here to download Electronic Supplementary Material \(for online publication only\): Supporting Information-Delaire et al.pdf](#)